Remote Sensing of Environment 240 (2020) 111675

Contents lists available at ScienceDirect

Remote Sensing of Environment

journal homepage: www.elsevier.com/locate/rse

Land surface phenology in the highland pastures of montane Central Asia: Interactions with snow cover seasonality and terrain characteristics

Monika A. Tomaszewska[a,c], Lan H. Nguyen[a,d], Geoffrey M. Henebry[b,c,*]

[a] Geospatial Sciences Center of Excellence, South Dakota State University, Brookings, SD 57007, USA
[b] Department of Geography, Environment, and Spatial Sciences, Michigan State University, East Lansing, MI 48824, USA
[c] Center for Global Change and Earth Observations, Michigan State University, East Lansing, MI 48823, USA
[d] Department of Biological Sciences, University of Calgary, Alberta, CANADA

ARTICLE INFO

Edited by Marie Weiss

Keywords:
Landsat
MODIS
Terrain effects
Kyrgyzstan
Climate change

ABSTRACT

Many studies have shown that high elevation environments are among very sensitive to climatic changes and where impacts are exacerbated. Across Central Asia, which is especially vulnerable to climate change due to aridity, the ability of global climate projections to capture the complex dynamics of mountainous environments is particularly limited. Over montane Central Asia, agropastoralism constitutes a major portion of the rural economy. Extensive herbaceous vegetation forms the basis of rural economies in Kyrgyzstan. Here we focus on snow cover seasonality and the effects of terrain on phenology in highland pastures using remote sensing data for 2001–2017. First, we describe the thermal regime of growing season using MODerate Resolution Imaging Spectrometer (MODIS) land surface temperature (LST) data, analyzing the modulation by elevation, slope, and aspect. We then characterized the phenology in highland pastures with metrics derived from modeling the land surface phenology using Landsat normalized difference vegetation index (NDVI) time series together with MODIS LST data. Using rank correlations, we then analyzed the influence of four metrics of snow cover seasonality calculated from MODIS snow cover composites—first date of snow, late date of snow, duration of snow season, and the number of snow-covered dates (SCD)—on two key metrics of land surface phenology in the subsequent growing season, specifically, peak height (PH; the maximum modeled NDVI) and thermal time to peak (TTP; the amount of growing degree-days accumulated during modeled green-up phase). We evaluated the role of terrain features in shaping the relationships between snow cover metrics and land surface phenology metrics using exact multinomial tests of equivalence. Key findings include (1) a positive relationship between SCD and PH occurred in over 1664 km^2 at $p < 0.01$ and 5793 km^2 at $p < 0.05$, which account for > 8% of 68,881 km^2 of the pasturelands analyzed in Kyrgyzstan; (2) more negative than positive correlations were found between snow cover onset and PH, and more positive correlations were observed between snowmelt timing and PH, indicating that a longer snow season can positively influence PH; (3) significant negative correlations between TTP and SCD appeared in 1840 km^2 at $p < 0.01$ and 6208 km^2 at $p < 0.05$, and a comparable but smaller area showed negative correlations between TTP and last date of snow (1538 km^2 at $p < 0.01$ and 5188 km^2 at $p < 0.05$), indicating that under changing climatic conditions toward earlier spring warming, decreased duration of snow cover may lead to lower pasture productivity, thereby threatening the sustainability of montane agropastoralism; and (4) terrain had a stronger influence on the timing of last date of snow cover than on the number of snow-covered dates, with slope being more important than aspect, and the strongest effect appearing from the interaction of aspect and steeper slopes. In this study, we characterized the snow-phenology interactions in highland pastures and revealed strong dependencies of pasture phenology on timing of snowmelt and the number of snow-covered dates.

1. Introduction

Studies have shown that high elevation environments are among the most sensitive to climatic changes (Diaz et al., 2003; Pepin et al., 2015; Thompson, 2000), where impacts are exacerbated (Chen et al., 2016; Immerzeel et al., 2010). Over Central Asia, which is especially vulnerable to climate changes (Lioubimtseva and Henebry, 2009; Luo et al., 2018; Yu et al., 2018), the ability of global climate projections to

* Corresponding author at: Department of Geography, Environment, and Spatial Sciences, Michigan State University, East Lansing, MI 48824, USA.
E-mail address: henebryg@msu.edu (G.M. Henebry).

https://doi.org/10.1016/j.rse.2020.111675
Received 11 August 2019; Received in revised form 19 December 2019; Accepted 19 January 2020
Available online 31 January 2020

capture the complex dynamics of mountainous environments is particularly limited (Reyer et al., 2017). There remains a scarcity of climate change impact studies for Central Asia (Hijioka et al., 2014; Xenarios et al., 2018).

In a semiarid, continental climate, agropastoralism constitutes the foundation of agriculture in montane Central Asia. According to FAO (Food and Agriculture Organization) statistics from 2015, rangelands constitute 87% of the agricultural land in Kyrgyzstan, the Central Asia country that is mostly mountainous (> 90% of land area) (FAO, 2015). Extensive herbaceous vegetation lands form a basis of rural economies in Kyrgyzstan, which makes the foundation of highlanders' livelihoods. For centuries, the herders of the highlands have been practicing vertical transhumance — the annual movement of livestock to higher elevation pastures to take advantage of seasonally available forage resources (Schillhorn Van Veen, 1995). Dependency on pasture resource availability during the short montane growing season makes herders susceptible to changes in climate and weather patterns.

In Central Asia, the Syr Darya and the Amu Darya are the region's major rivers that flow into the Aral Sea Basin (Bernauer and Siegfried, 2012). River flow is driven by meltwater from glaciers and snow cover in the Tien Shan and Pamir mountains as well as runoff from across the basin (Sorg et al., 2012). Increasing temperatures trigger accelerated glacier mass loss and snow cover shrinkage, and projected warming is expected to affect significantly melt characteristics as timing and magnitude (Luo et al., 2018; Wang et al., 2014). Melt characteristics are particularly important, since seasonal and longer-term water storage are critical ecosystem services provided by mountains, especially in drier climates (Immerzeel et al., 2010). Recent studies over the region have shown a shift in precipitation from snow to rain, which decreases snowfall fraction and results in less accumulation of snow and glacier ice during the winter (Chen et al., 2016). Moreover, changes in snow cover and shrinkage of glaciers lead to alterations in the local water cycle and water storage (Bai et al., 2019; Dedieu et al., 2014). While increased temperatures may result in an extended growing season that could benefit certain vegetation types and communities, enhanced variation in rainfall and snowfalltiming and amount of water availability (Chen et al., 2016; Immerzeel et al., 2010), and increased incidence of drought may negatively affect vegetation phenology and pasture productivity (Marshall et al., 2019; Petersky et al., 2019).

Snowfall dominates the annual precipitation total in montane Central Asia (Aizen et al., 1995; Apel et al., 2018; Sorg et al., 2012); thus, changes in timing and/or magnitude could be especially consequential, since snowmelt is the main contributor to early growing season soil moisture, and most of the seasonal biomass accumulation in pastures relies on this initial store of moisture. Variation in the duration of snow cover and snow depth may affect soil-vegetation interactions. Increased snow cover duration and/or depth could add soil moisture, slow down soil heat exchange, and have crucial effects on soil heat and moisture preservation that might protect over-winter survival of vegetation from low air temperatures and wind damage. It may also affect the activity of soil microbes and the transformation of soil organic matter and nutrients (Groffman et al., 2001; Qiao and Wang, 2019). Deeper snow depths may lead to later start of phenology, which in turn might not be beneficial for soil respiration over winter or the accumulation of heat needed to unfold leaves in spring (Monson et al., 2006; Schimel et al., 2004). However, Welker et al. (2005) showed that deeper snow could alter carbon-to-nitrogen (C:N ratios) leading to increased N in leaves that may result in higher crude protein content in forage. Earlier snow cover could shield vegetation from lower temperatures by keeping the subniveal temperature at a favorable level and protecting the activity of the soil microorganisms during the winter, which could lead to increased vegetation growth during the following growing season. On the other hand, lack of snow cover or just a shallow snowpack may increase the frequency of soil freeze-thaw events and, consequently, alter soil nutrient cycling and aboveground productivity (Choler, 2015).

Here we address three open questions regarding snow cover seasonality and terrain effects on pasture phenology:

(1) How does snow cover seasonality relate to subsequent land surface phenology in highland pastures?
(2) How does mountainous terrain modulate snow cover effects?
(3) What can recent changes in snow cover seasonality tell us about possible futures for highland pasture phenology and productivity?

There are recent studies that analyze snow cover impact on pasture phenology using remote sensing products over specific regions in Central Asia and High Mountain Asia. Paudel and Andersen (2013) explored the response of rangeland vegetation to snow cover dynamics in Nepal Trans Himalayas; whereas, Wan et al. (2014) explored relationships between changes in snow cover and its impact on alpine vegetation in Qinghai-Tibetan Plateau. More recently, Wang et al. (2018) studied snow cover effects on alpine vegetation growth dynamics over Tibetan Plateau. Relationships between winter snow cover dynamics, climate, and spring grassland phenology in Inner Mongolia, China was analyzed by Qiao and Wang (2019). Each study found changes in snow cover affecting the length of the growing season and, especially, the start of the growing season, which also influences aboveground net primary production as viewed through the normalized difference vegetation index (NDVI) (Tucker, 1979).

Due to the scarcity of ground-level data, an inability to access much data from the Soviet era, and the fact that most weather stations are located in valleys far from the pastures of interest, we relied on remote sensing datasets for measurement and indicators of snow and pasture phenology.

We framed this study using three key aspects of the highland environment (thermal regime, moisture regime, and terrain attributes) that drive and constrain the growth and development of pasture vegetation. Here we describe the thermal regime of growing season using MODIS Land Surface Temperature (LST) dataset and analyze how it is modulated by mountainous terrain. The moisture regime and its changes have already been described using snow cover metrics and trends in snow cover seasonality (Tomaszewska and Henebry, 2018). The study period corresponds to the MODIS era: 2001–2017, and the study area encompasses pastures across Kyrgyzstan.

First, we explored pasture phenology characteristics *via* modeling of land surface phenology (LSP) by combining Landsat surface NDVI and MODIS LST data. Phenological modeling has previously provided evidence of changes in land surface dynamics and phenology in Central Asia (Bohovic et al., 2016; de Beurs et al., 2015, 2018; de Beurs and Henebry, 2008; Kariyeva and van Leeuwen, 2011; Lu et al., 2014).

Second, we analyzed the influence of snow cover seasonality on the phenological development in pastures using both Spearman's rank correlation and asymmetry analysis.

Finally, we investigated the role of terrain features—elevation, slope, and aspect—in modulating the thermal regime and in shaping relations between snow cover and subsequent phenology and productivity in highland pastures. Each of those steps prepared us to address the bigger picture of pasture vegetation dynamics to identify where in the landscape of pastures the phenology were more sensitive to variable and changing climatic conditions. Pastures are for grazing animals, but we did not explicitly address grazing dynamics in this synoptic study because (1) vertical transhumance is the key livestock management technique in these agropastoralist communities and (2) we were addressing all pasture areas across the country without regard to the seasonality of use.

2. Study area

The study area falls within the territory of Kyrgyzstan (Kyrgyz Republic), a land-locked republic in Central Asia. A highly mountainous country, it is bordered on the north and northwest by Kazakhstan, on

the east and southeast by China, on the southwest by Tajikistan, and on the west by Uzbekistan. With a population of about 6 million, the total area of Kyrgyzstan is 199,951 km^2, of which nearly 96% is land with 8150 km^2 in lakes and reservoirs (WorldBank, 2018). More than 56% of the territory lies above 2500 m, where mountains ranges of the Tien Shan, the Pamir, and the Alatau cover > 90% of the total land area (Azykova, 2002). The country is divided into seven *oblasts* or provinces—Talas, Chuy (including the capital Bishkek), and Issyk-Kul on the northern part of the country, and Jalal-Abad, Naryn, Osh, and Batken in the southern part—and 40 *rayons* or districts (Asian Development Bank, 2010a).

The climate of Kyrgyzstan is continental with low precipitation and intense solar radiation. Weather patterns are influenced by the high elevation, mountain ranges, distance from oceans, adjacency to the deserts, and the country's inland location in the temperate and subtropical zone (Akimaliev et al., 2013). Due to the high relief of the terrain, there is significant geographic and interannual variation in daily and seasonal averages of air temperature and moisture, which result in climatic zonation by elevation. During summer months (June through August) the average air temperature can reach from 17 to 40 °C over lowlands, while dropping to −4 °C in the mountains. The lowest average air temperatures during winter are registered in the high mountain valleys; whereas, frost occurs over the entire country (Kulikov and Schickhoff, 2017). Precipitation is unequally distributed across the country, with the lowest annual precipitation of < 150 mm in some areas of Issyk-Kul oblast in northeastern Kyrgyzstan to > 1000 mm over the lowlands of the Ferghana valley to the west. More than 50% of the land area is used as pastoral rangelands, which constitutes 87% (according to FAO, 2015 statistics) of the agricultural lands in Kyrgyzstan. Less than 10% of the land is suitable for crops, while forests cover only about 5%. Our focal areas are the pastures of Kyrgyzstan, and our study period extends from 2000/2001 to 2017 (Fig. 1).

3. Geospatial data

3.1. MODIS snow cover product

We used the most recent version of the MODIS Terra snow cover 8-day composites (MOD10A2 V006; Riggs and Hall, 2015) distributed by the National Snow and Ice Data Center (https://nsidc.org/). The nominal spatial resolution is 500 m, and the data are provided in a sinusoidal projection. MOD10A2 product reports the maximum snow cover extent observed during 8-day period by compositing observations from the MODIS/Terra Snow Cover Daily L3 Global 500 m Grid product (MOD10A1 V006), where the snow cover information is derived using the Normalized Difference Snow Index (NDSI) (Hall et al., 2002; Riggs and Hall, 2004). The annual dataset contains 46 8-day composites. We downloaded two MODIS tiles (h23v04 and h23v05) from 2000 to the end of 2017, resampled them to 30 m using nearest neighbors.

3.2. MODIS land surface temperature products

We used the MODIS/Terra and MODIS/Aqua Land Surface Temperature/Emissivity products at 1 km spatial resolution (M{O|Y}D11A2 V006), which provide an average 8-day land surface temperature (LST) for all M{O|Y}D11A1 LST pixels collected within the 8-day time frame (Wan et al., 2015). We downloaded two MODIS tiles (h23v04 and h23v05) of MODIS/Terra from 2001 and MODIS/Aqua from 2002 through the end of 2017. We resampled the data to 30 m pixel resolution using bilinear resampling. We created a second dataset in which we left the spatial resolution at the nominal 1 km. This second dataset was used to characterize the thermal regimes as a function of terrain (*cf.* Sections 4.2, 5.1, and 6.1). In contrast, the first dataset was used for land surface phenology modeling (*cf.* Sections 4.3, 5.2, and 6.2).

3.3. Landsat surface reflectance products

We worked with the Landsat Collection 1 Tier 1 Level-1 Precision

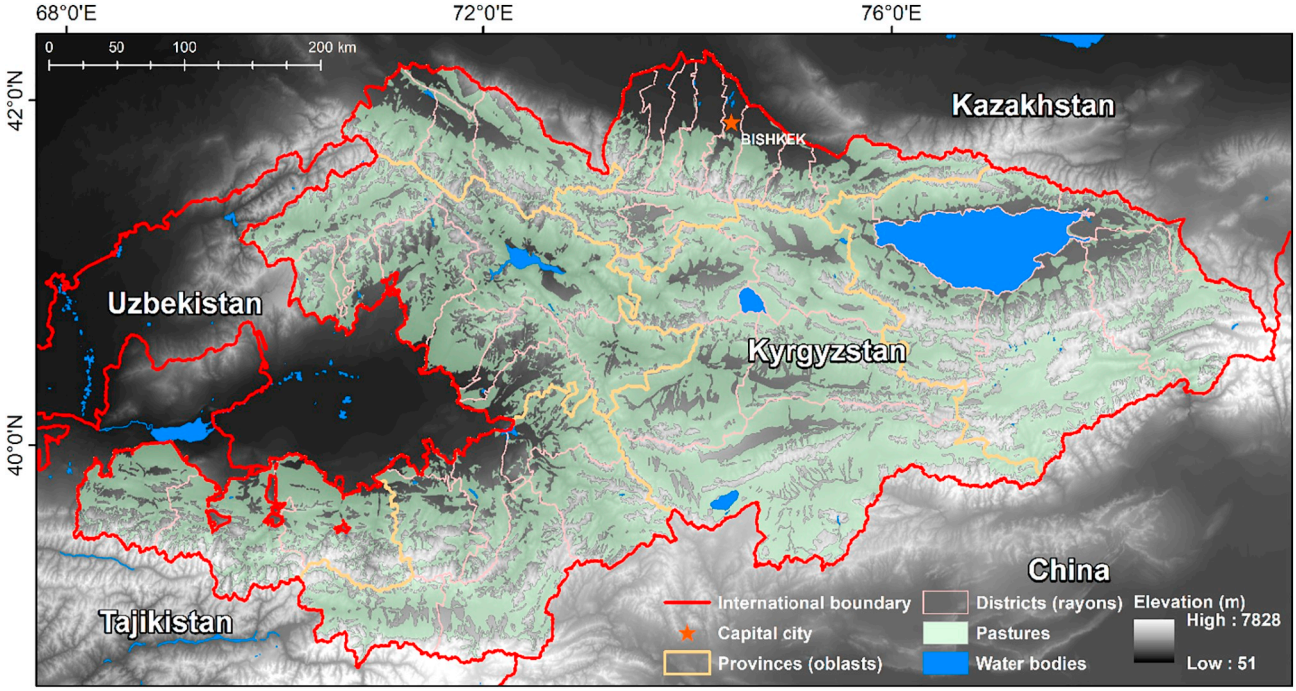

Fig. 1. Study area: pasture land use in Kyrgyzstan is displayed in light green from (Asian Development Bank, 2010a, 2010b) and draped over the SRTM 30 m Digital Elevation Model (DEM) (Projected coordinate system: Albers Conic Equal Area). (For interpretation of the references to colour in this figure legend, the reader is referred to the web version of this article.)

and Terrain (L1TP) corrected product from 2001 to the end of 2017 that is generated from Landsat 8 Operational Land Imager (OLI), Landsat 7 ETM+, and Landsat 5 Thematic Mapper (TM) (USGS EROS, 2017). Surface reflectance NDVI data were obtained by downloading 13,285 images in 33 tiles (WRS-2 Paths 147 to 155 and Rows 30 to 33; Table A1) from the USGS Earth Resources Observation and Science (EROS) Center Science Processing Architecture (ESPA) On Demand Interface (https://espa.cr.usgs.gov/). We used an inter-calibration equation to adjust Landsat 7 ETM+ surface NDVI and Landsat 5 TM surface NDVI to the surface Landsat 8 OLI NDVI, which on average has higher values (Roy et al., 2016):

$$NDVI_{OLI} = 0.0235 + 0.9723 \times \{NDVI_{TM} \mid NDVI_{ETM+}\} \quad (1)$$

We used Eq. (1) on both datasets since the differences between surface NDVI from Landsat 7 ETM+ and Landsat 5 TM are very small. Moreover, these datasets have been used together successfully in studies of land surface phenology (*e.g.*, Fisher et al., 2006; Melaas et al., 2013).

In areas with terrain complexity, differential illumination remains a controlling factor on the radiometric properties of remotely sensed data. The difference of illumination and variation of the proportion of light reflected from the ground to the sensor may yield variable spectral responses even in homogeneous land covers (Allen, 2000; Vázquez-Jiménez et al., 2017). Based on exploratory analysis (*cf.* Appendix A), we concluded a topographic normalization method was not necessary, given our questions and the demonstrated ability of the NDVI to attenuate a large amount of the variation induced by changing sun angles, topography, clouds or shadows, and atmospheric conditions (Huete et al., 1999; Matsushita et al., 2007).

3.4. Other geospatial data

For representation of the terrain, we used two digital elevation datasets. At the finer resolution, we used the SRTMGL1, the NASA Shuttle Radar Topography Mission Global 1 arc-second (~30 m) V003 product (NASA JPL, 2013). We downloaded 133 tiles from USGS Earth Explorer (https://earthexplorer.usgs.gov/) and resampled them to 30 m spatial resolution. Further, we generated two layers—slope (in degrees) and aspect (in degrees)—and reclassified them into groups for subsequent analysis: five slope classes (0–5°, 5–10°, 10–15°, 15–30°, > 30°), and nine aspect classes (N, NE, E, SE, S, SW, W, NW, and flat).

The second was the Global Multi-resolution Terrain Elevation Data 2010 (GMTED2010) mean product at 30 arc-seconds (~1 km) developed by the US Geological Survey and the National Geospatial-Intelligence Agency (Danielson and Gesch, 2011). We l resampled the data to 1 km using bilinear resampling. We again created two layers—slope (in degrees) and aspect (in degrees)—and reclassified them into groups: four slope classes (0–5°, 5–10°, 10–15°, 15–30°) and just two aspect classes for aspect: Northern (NE + N + NW) and Southern (SE + S + SW). Due to its coarser spatial resolution, there is no > 30° slope class in the GMTED2010.

Pasture land use information was obtained from a Soviet-era land use map that was updated in 2008 using Landsat 7 ETM+ images and MODIS datasets for the CACILM project (Asian Development Bank, 2010a, 2010b).

4. Methods—data processing

Fig. 2 offers an overview of the study's technical workflows to aid navigation of the multitude of data and multiple analysis steps.

4.1. Metrics of snow seasonality

We described snow seasonality by generating four temporal metrics for each snow season. We defined our observation window to bound the snow cover season each year by starting on the day of year (DOY) 169 (approximately the summer solstice) and extending to DOY 168 in the following year ($DOY169_{year}$ through $DOY168_{year+1}$). This approach enabled us to identify the first and last appearances of snow cover during the cold season. We generated four snow cover metrics: First Date of Snow (FDoS), Last Date of Snow (LDoS), Duration of Snow Season (DoSS), and the number of Snow-Covered Dates (SCD). FDoS is the composite date when the pixel is flagged as snow for the first time each snow cover season. LDoS is, conversely to FDoS, the last composite date with pixel marked as snow in each of the snow season. DoSS is the difference in composite dates between LDoS and FDoS multiplied by 8 to align with DOY [(LDoS – FDoS + 1)*8]; SCD is a number of composites with snow cover present between FDoS and LDoS, also multiplied by 8 (Tomaszewska and Henebry, 2018).

We used 8-day composites rather than daily data to obtain consistent statistical power across trend analyses, a significant advantage over daily time series.

Fig. 3 illustrates the mean LDoS across 17 years of observations across those pasture areas with at least one year of successful LSP fitting.

The earlier mean LDoS during the snow season occurs mostly over western lowlands near the Ferghana Valley, in the interior at lower elevations, and around Issyk-Kul (the large lake of the endorheic basin in northeastern Kyrgyzstan). The latest snowmelt occurs at higher pastures in central Kyrgyzstan, and over the southern and southeastern parts of the Tien-Shan mountains. The average snow-covered dates appear in Fig. 4. Higher values of SCD occur over the southern area of the country, close to the northern range of the Pamirs, and over the higher ridges of the Tien-Shan in central Kyrgyzstan. The least SCD occur at the edges of the Ferghana Valley, and along the lower elevated areas around Issyk-Kul. See Appendix for the maps of mean FDoS (Fig. A1) and mean DoSS (Fig. A2).

4.2. Metrics of thermal time

We calculated accumulated growing degree-days (AGDD) to characterize the progression of thermal time during the year. Growing degree-days (GDD) can be interpreted as a proxy of insolation, potentially useful for growth and development of herbaceous vegetation in the temperate mid-latitudes (de Beurs and Henebry, 2010a; Henebry, 2013). We modified an algorithm developed by Krehbiel and Henebry (2016), and subsequently revised (Krehbiel et al., 2017; Nguyen et al., 2018) to calculate AGDD from MODIS LST time series. The transformation of two daytime and nighttime observations from Terra and Aqua into mean MODIS LST was based on Eq. (2), where the highest and the lowest LST values were selected to calculate the mean MODIS LST:

$$\text{mean MODIS LST} = [\max(LST_{1030}, LST_{1330}) + \min(LST_{2230}, LST_{0130})]/2 \quad (2)$$

For the year 2001 and part of 2002, we used only MODIS/Terra images. To fill gaps due to missing or excluded pixels by filtering, we used the Seasonally Decomposed Missing Value Imputation approach (Moritz and Bartz-Beielstein, 2017). We further filtered out mean MODIS LST below 0 °C, and calculated the GDD Eq. (3) at composite period t as the maximum between mean LST and T_{base}, which was set to 0 °C (Goodin and Henebry, 1997; Henebry, 2013). Each of 46 GDD composites was multiplied by 8 to account for the 8-day compositing time frame of the MODIS product, and then accumulated for each of 17 years Eq. (4).

$$GDD_t = \max((\text{mean MODIS } LST_t - T_{base}), 0) \quad (3)$$

$$AGDD_t = AGDD_{t-1} + (GDD_t \times 8) \quad (4)$$

Fig. 5 illustrates the average annual AGDD across the pasture areas of Kyrgyzstan. Note the higher mean AGDD (in reds) occur over western

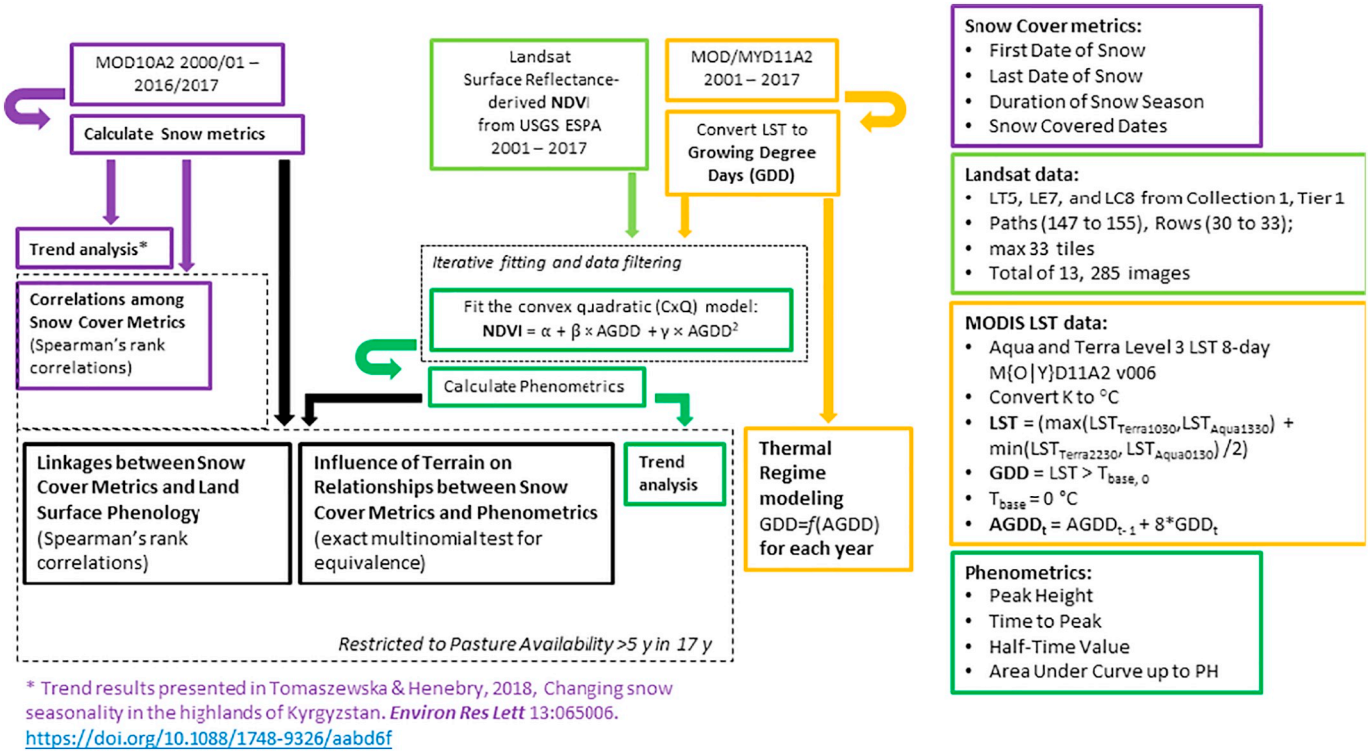

Fig. 2. Overview of technical workflows.

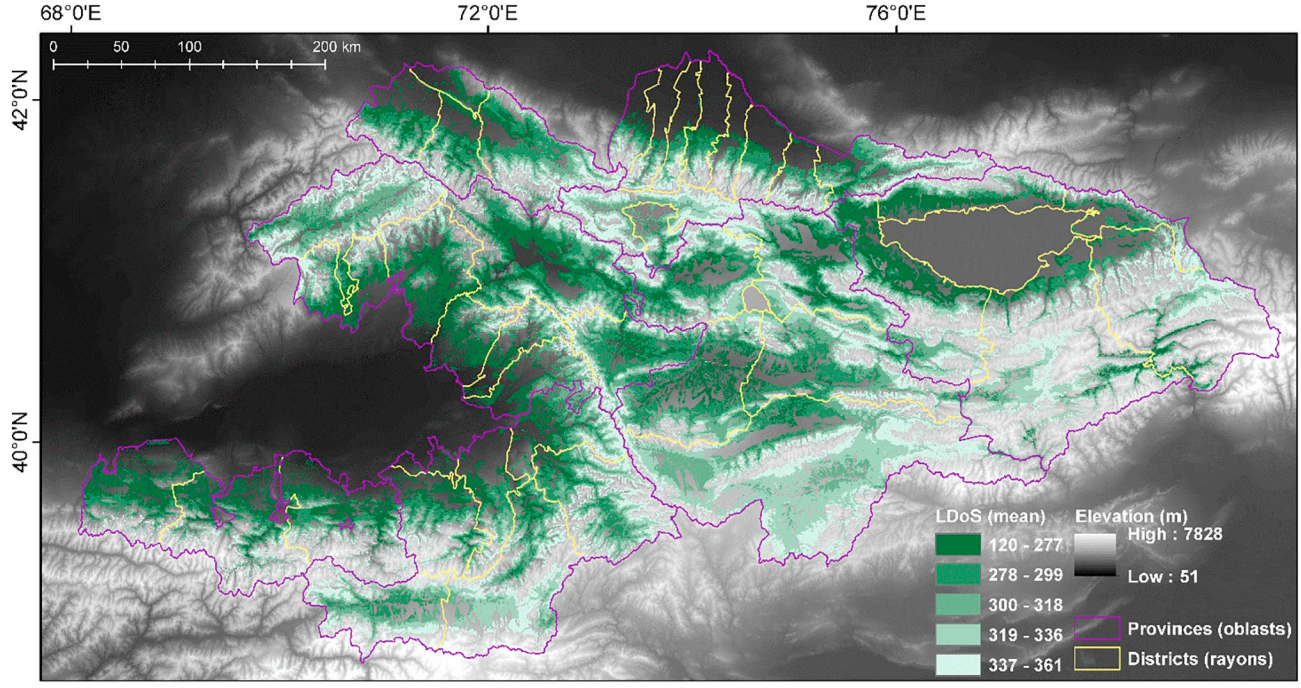

Fig. 3. Mean values of Last Date of Snow (LDoS). Note that those values refer to the snow season range from 1 to 361 using MODIS 8-day composites. Thus, value 361 is equivalent to DOY161$_{year+1}$ using the MODIS 8-day composites naming convention. Map draped over the SRTM 30 m DEM displays data only for pasture land use (Projected coordinate system: Albers Conic Equal Area).

lowlands near the Ferghana Valley in Uzbekistan, in the interior of the country at lower elevations, and around Issyk-Kul. The lowest average AGDD (in blues) occur over southern Kyrgyzstan, which has higher elevations.

4.3. Land surface phenology

We used a downward-arching convex quadratic (CxQ) function to model LSP (de Beurs and Henebry, 2004; de Beurs and Henebry, 2010a; Henebry and de Beurs, 2013) as follows:

$$NDVI = \alpha + \beta \times AGDD + \gamma \times AGDD^2 \quad (5)$$

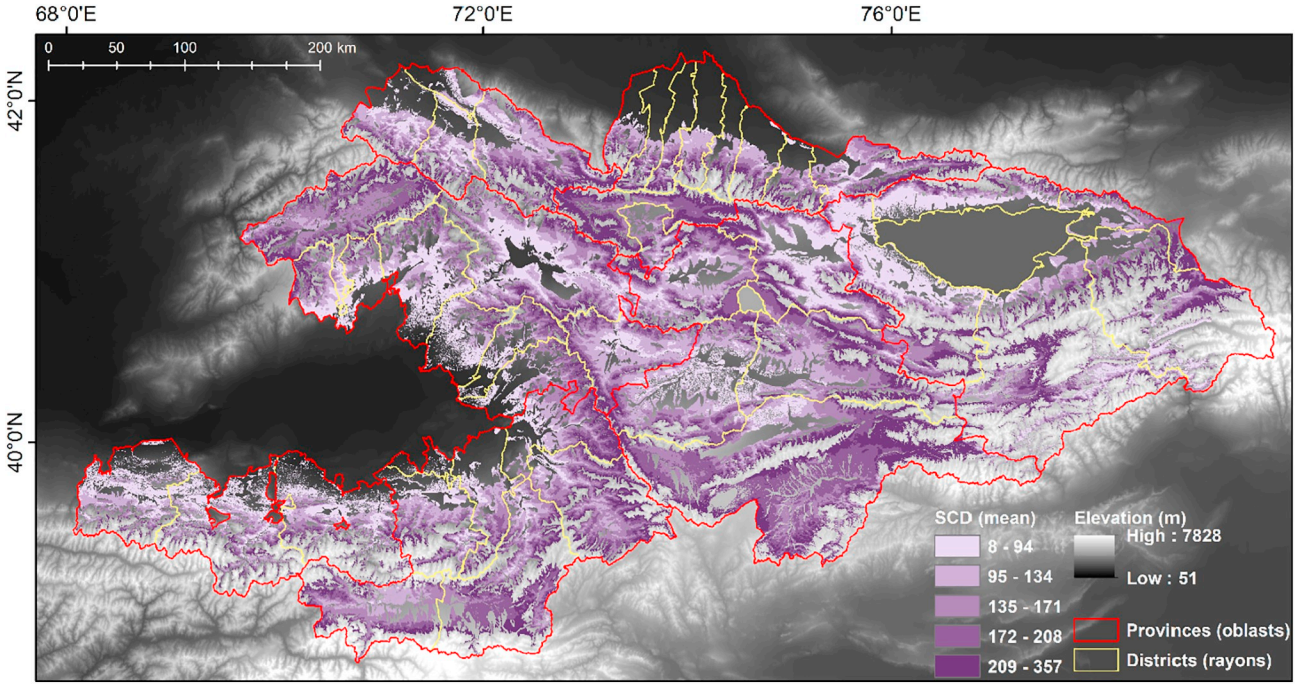

Fig. 4. Mean values of Snow Cover Dates (SCD). Map draped over the SRTM 30 m DEM display data only for pasture land use (Projected coordinate system: Albers Conic Equal Area).

where the fitted coefficient of the quadratic parameter (γ) was required to be negative. Landsat surface reflectance data served to calculate NDVI as a proxy for active green vegetation, and MODIS LST for AGDD as a proxy for insolation, since the land surface temperature in grasslands during the growing season is highly correlated with insolation (Henebry, 2013; Still et al., 2014).

For each pixel in the study area, we used the fitted parameter coefficients—intercept (α), slope (β), and quadratic (γ)—to calculate four phenological metrics (phenometrics) for each year from 2001 to 2017. These phenometrics provide indications of pasture condition (Table 1).

It was necessary to filter the pixel time series to reduce noise and spurious data prior to model fitting and then to evaluate the quality of each fit. For each period spanning the 8-day AGDD composites, we used the corresponding Landsat observation with the highest NDVI value. We filtered out observations with NDVI $<$ 0.1 and AGDD $<$ 100 to avoid including non-vegetated or snow-covered pixels. In addition, to account for cloud contamination that might not have been eliminated

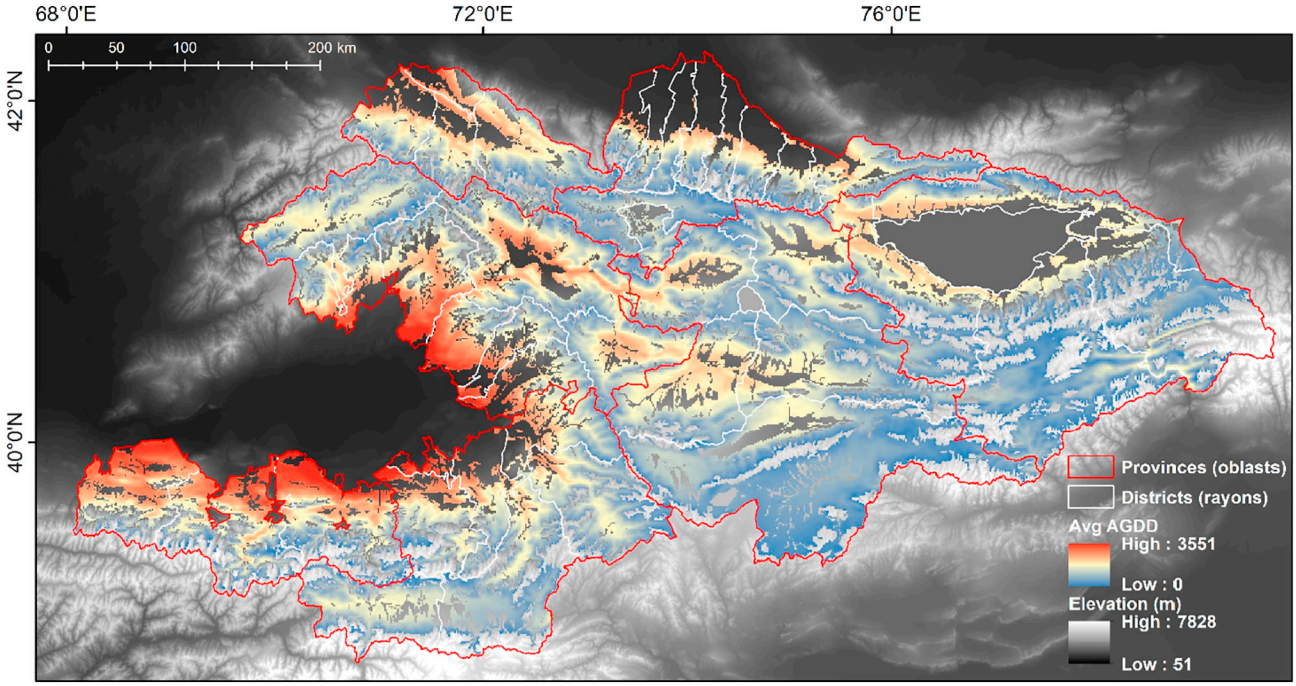

Fig. 5. MODIS LST-derived (2001–2017) mean annual AGDD (°C) for pasture land use in Kyrgyzstan. Map draped over the SRTM 30 m DEM displays data only for pasture land use (Projected coordinate system: Albers Conic Equal Area).

Table 1
Phenology metrics (phenometrics) used in the study.

Phenometrics	Equation	Description
Peak Height	$PH = \alpha - (\beta^2 / 4\gamma)$	the maximum modeled NDVI
Thermal Time to Peak	$TTP = -\beta / 2\gamma$	the quantity of AGDD required to reach PH; corresponds to duration of modeled green-up phase
Half-Time Value	$HTV = \alpha - (3\beta^2) / (16\gamma)$	NDVI at half-TTP; corresponds to green-up rate
Area Under the Curve up to PH and TTP	$AUC = \Sigma_{i=1,t} (NDVI_t + NDVI_{t-1}) / 2 \times (AGDD_t - AGDD_{t-1})$	numerically integrating by trapezoidal method the NDVI time series as a function of thermal time, serves as a proxy of pasture productivity during the green-up phase

through quality masking, we looked for unusual dips in the NDVI time series. We first calculated the simple average of NDVI observations on either side of the focal observation. We then calculated the percentage difference between the average NDVI and the focal observation, and then excluded observations that were greater than or equal to 15% than the average of the two neighboring observations.

For each pixel in each year, we fitted the filtered NDVI and associated AGDD time series to the downward-arching CxQ LSP model shown in Eq. (5). We accepted the fitted model—specifically, its fitted parameter coefficients—for further analysis only if it passed all six of the following criteria that we used to control fitting performance:

(1) the quadratic parameter (γ) was < 0;
(2) at least seven observations, where three observations were distributed before and at least three after the PH;
(3) the TTP greater than the AGDD of the first observation;
(4) the adjusted $R^2 > 0.7$;
(5) the Root Mean Square Difference (RMSD) < 0.08; and
(6) the PH below 1.0.

If any criterion was not fulfilled during the fitting, then the last observation was removed from the filtered dataset, and the model fitting was rerun over the newly filtered dataset. We repeated this fitting procedure until either the fitted model passed all criteria or the length of the time series was fewer than 7 observations. In the latter case, the model fit for that pixel was labeled a failure in that year and no phenometrics were calculated. Finally, for the successfully fit models, we calculated the AUC up to PH using a baseline of AGDD = 100 and NDVI = 0.10 using trapezoidal integration. Fig. A3 shows the total number of observations over 17 years used for successful fits.

5. Methods—data analysis

5.1. Thermal regime of growing season

To understand thermal regime of the growing season over pasture areas over Kyrgyzstan, we fitted mean GDD values for 1000 randomly selected pixels as a quadratic function of AGDD (at 1 km spatial resolution) varying by elevation, slope gradient (in four classes: 0–5°, 5–10°, 10–15°, 15–30°), and contrasting aspects (northern: NE + N + NW, southern: SE + S + SW). We used fitted parameter coefficients of quadratic curves from modeling and calculated PH for GDD and TTP for AGDD.

5.2. Land surface phenology

We summarized each annual fit with a binary variable (0 = no fit, 1 = fit) to generate a final map of the total number of years with successful fits for each pixel. Then we divided these results into three pasture availability classes: (i) Highly Persistent (HP) pastures with 11–17 years of successful fits out of 17 years of observations, (ii) Persistent (P) pastures with 5–10 years, and (iii) Rarely Available (RA) pastures with just 1–4 years of successful fits. We based all subsequent analyses only on those pixels in either the HP or P pasture availability classes, because these locations host the natural resources that provide the foundation of the pastoralist economy.

Based on the successful model fits, we calculated basic descriptive statistics (mean, standard deviation, and coefficient of variation) for each of the four phenometrics (*viz.*, PH, TTP, HTV, and AUC) for the series of 17 seasons from 2001 through 2017.

5.3. Spearman's rank correlation to link snow cover seasonality with phenometrics

To estimate the association of the metrics of snow cover seasonality with phenometrics from the subsequent growing season, we used Spearman's rank correlations (Fieller et al., 1957; Lehmann and D'Abrera, 2006), which assesses whether a monotonic relationship—not necessarily linear—occurs between two variables. The method is robust against outliers and works for data exhibiting non-normality. We used rank correlations in two ways: (1) to evaluate the relationships among the four snow cover temporal metrics (*viz.*, FDoS, LDoS, DoSS, and SCD); and (2) to evaluate the relationships between the four snow cover temporal metrics and four phenometrics (*viz.*, TTP, PH, HTV, AUC) for the Highly Persistent (HP) and Persistent (P) pasture availability classes, separately. We calculated the areal percentage of pixels exhibiting significant positive or negative correlations at $p < 0.01$ and $p < 0.05$, and the ratio of pixels with positive correlations to pixels with negative correlations to identify the predominant direction of the detected significant relationships. We used threshold values of > 2.0 to indicate a strong asymmetry favoring significant positive correlations and of < 0.5 to indicate a strong asymmetry favoring significant negative correlations.

5.4. Exact test for multinomial equivalence of terrain effects

Statistical tests of the difference (inequality) are typically used in remote sensing studies to determine whether differences between groups are statistically significant (Foody, 2009). Here we instead conducted a series of equivalence tests to evaluate the influence of terrain on the associations between snow seasonality and phenometrics, due to the very large sample size and non-negligible spatial autocorrelation (de Beurs et al., 2015; Foody, 2009; Frey, 2009; Wellek, 2010).

H_0: $d(p, p0) \geq \Delta$ against H_1: $d(p, p0) < \Delta$

where d(p,p0) is the observed Euclidean distance between two probability densities (distributions), the 95% upper bound for d(p,p0) corresponds to a p-value of 0.05, Δ is a threshold distance between distributions Posed another way: if the distance between the two distributions is less than Δ (*viz.*, failing to reject both one-sided tests), then we conclude the distributions are equivalent. We used a conservative version of the exact multinomial test for equivalence since the sample sizes were large, and we selected $\Delta = 0.025$ as the standard for equivalence (Frey, 2009).

To investigate the influence of terrain on the linkage between snow cover seasonality and land surface phenology, we delineated nine areas in HP pastures where spatial clusters of significant correlations between

particular snow cover temporal metrics and phenometrics were evident (Fig. A4), and called them hotspots. The null hypothesis for our equivalence testing is that terrain plays a major role in shaping the relationship between snow cover seasonality and the phenometrics in the subsequent warm season in that hotspot. Rejecting H_0 deems the two distributions as equivalent, indicating that no effect of the terrain feature is evident.

For each hotspot, we calculated the proportions of pixels over the entire area hosting the hotspot in different terrain feature classes. These data were the "potential" distribution. We also calculated the proportion of pixels exhibiting significant correlations between the snow cover temporal metrics and the phenometrics in different terrain feature classes. This subset of pixels was the "observed" distribution. We tabulated proportions in aspect in nine classes, slope in five classes, and slope × aspect interactions, giving a total of eight terrain feature groups: aspect; slope; 0–5° × aspect; 5–10° × aspect; 10–15° × aspect; 15–30° x aspect; > 30° × aspect; and slope × aspect. For each terrain feature group, we ran a separate exact multinomial test for equivalence. We generated "observed" distributions as follows: for positive correlations between SCD and PH for nine hotspots; positive correlations between LDoS and PH for hotspots 1–8; negative correlations between LDoS and PH for hotspot 9 only; and, for all nine hotspots, negative correlations between SCD and TTP, negative correlations between LDoS and TTP; and positive correlations between SCD and HTV.

6. Results

6.1. Thermal regimes of the warm season

Thermal regimes in highland pastures can be summarized by the shape of GDD as a function of AGDD changes due to elevation (Fig. 6). It is clear from Fig. 6 and from Table 2 that (1) the patterns of GDD as a function of AGDD during the warm season are well-approximated by the same kind of downward-arching parabolic shape used to model LSP, and (2) the seasonal amplitudes (PH_{GDD}) and durations (TTP_{AGDD}) change smoothly as a function of elevation. PH_{GDD} and TTP_{AGDD} are greater at the lower elevations (Table 2). The annual variation represented by the error bars (± 2 SEM) across the 17 years of observation is much higher during beginning and end of the warm season than the seasonal peak at lower elevations; however, at higher elevations, variation is much larger just before peak values (Fig. 6). Some asymmetries in the seasonal curves are evident and documented by the pattern of adjusted R^2 values, which reach a relative low point in the 2400–2900 m elevation class (Table 2).

Table 2
Modeled PH and TTP, adjusted R^2 values on GDD – AGDD quadratic curve at different elevation ranges.

Elevation class (m)	PH_{GDD}	TTP_{AGDD}	Adjusted R^2	$AGDD_{max}$
< 1800	29.5	2527	0.94	4961
1800–2400	23.1	1774	0.92	3491
2400–2900	18.8	1313	0.91	2576
2900–3400	15.3	937	0.92	1833
3400–4000	11.9	625	0.94	1236
> 4000	8.8	392	0.95	779

Fig. 7 shows the mean annual progression of thermal time during the warm season as a function of both slope and aspect for the six elevation classes. Four patterns are notable. First, at the beginning of the warm season there is very little distinction in the progression of thermal time among terrain features. As the season progresses, divergence among slope × aspect classes becomes more pronounced. Second, the divergences between contrasting aspects (northern *vs.* southern) are more pronounced in steeper slope classes. Third, interactions of slope and aspect result in virtually interchangeable thermal time profiles, especially at higher elevations, but these interactions can produce counter-intuitive results. Two examples: (1) in the 2900–3400 m class, the southern aspect pixels on 15–30° slopes (open yellow) show a comparable seasonal profile to the northern aspect pixels on 0–5° slopes (solid black); and (2) in the 3400–4000 m class, the southern aspect pixels on 5–10° slopes (open magenta) track similarly to northern aspect pixels on 15–30° slopes (solid yellow).

6.2. Land surface phenology

We obtained 115,551,865 pixels (103,997 km^2) in successful model fits over pasture areas for the 17-year period. This total pixel area corresponds to 52% of the country's land area and 85% of the pasture land use area. Highly Persistent (HP) pastures covered 15,261 km^2 or 12.5% of pasture land use area, Persistent (P) pastures covered 53,620 km^2 or 43.8% (Fig. 8). The total area of unsuccessful fits covered 18,412 km^2 or 15% of pasture land use. Table 3 shows the

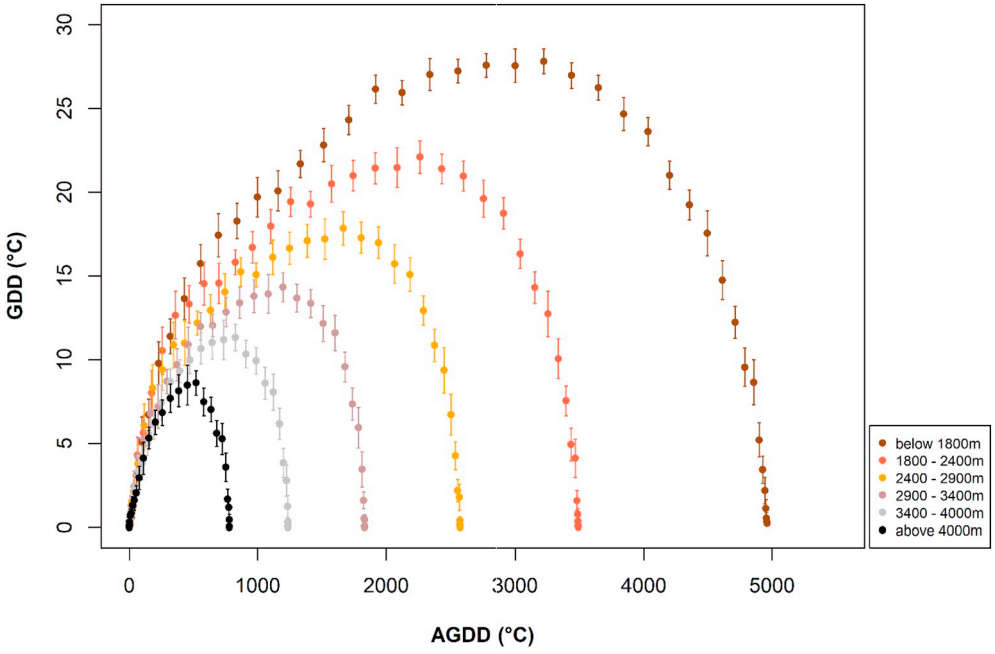

Fig. 6. Mean annual Growing Degree-Days (GDD) with ± 2 SEM (Standard Errors of Mean) *vs.* mean annual Accumulated Growing Degree-Days (AGDD) for 1000 randomly selected pixels within six elevation classes: (i) below 1800 m (brown), (ii) 1800–2400 m (orange), (iii) 2400–2900 m (golden), (iv) 2900–3400 m (rosy brown), (v) 3400–4000 m (gray), and (vi) above 4000 m (black). (For interpretation of the references to color in this figure legend, the reader is referred to the web version of this article.)

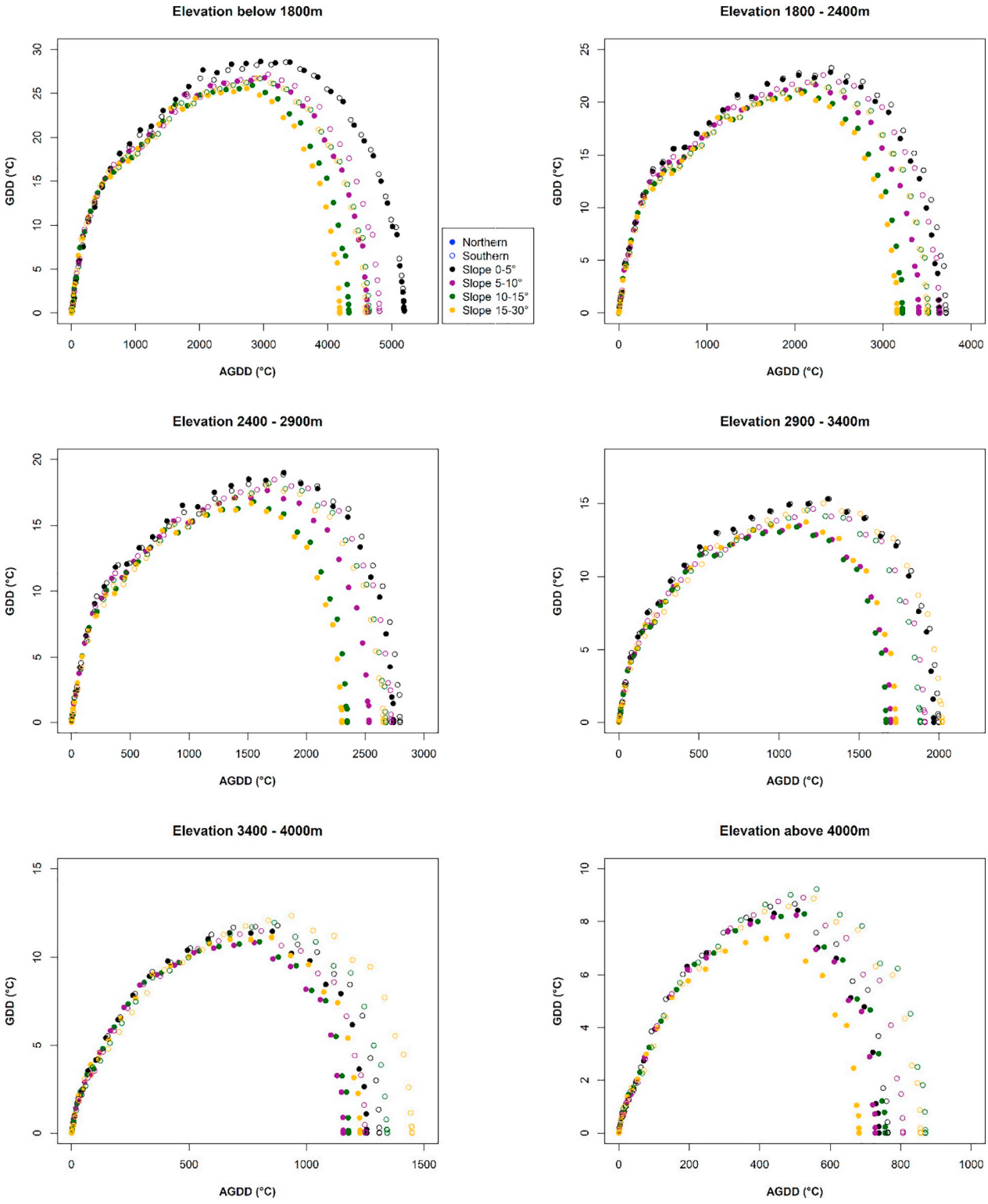

Fig. 7. Mean annual Growing Degree-Days (GDD) *vs.* mean annual Accumulated Growing Degree- Days for 1000 randomly selected pixels at six elevation ranges: (i) below 1800 m, (ii) 1800–2400 m, (iii) 2400–2900 m, (iv) 2900–3400 m, (v) 3400–4000 m, and (vi) above 4000 m, for northern (filled circle) and southern (open circle) aspects at four slope classes: (i) 0–5°, (ii) 5–10°, (iii) 10–15°, (iv) 15–30°. Note that the scaling of the y-axes varies between panels.

distribution of pasture availability classes by elevation in areal percentage (including Rarely Available (RA) that were excluded from subsequent analyses). In Fig. 8, note the purple stripes that arise, in part, from increased observations available in those stripes. While it is not possible to disentangle data availability from *in situ* pasture suitability, the segregation of the pixels into different temporal classes helps to focus the subsequent analyses of linkages between variables to locations with more data.

Highly persistent pastures are prevalent from 1800 to 2400 m, with nearly one-third found between 2400 m and 2900 m and 27% from 1800 m to 2400 m. In contrast, there are more persistent pastures above 2900 m and roughly the same proportion below 2400 m: 43% in HP *vs.*

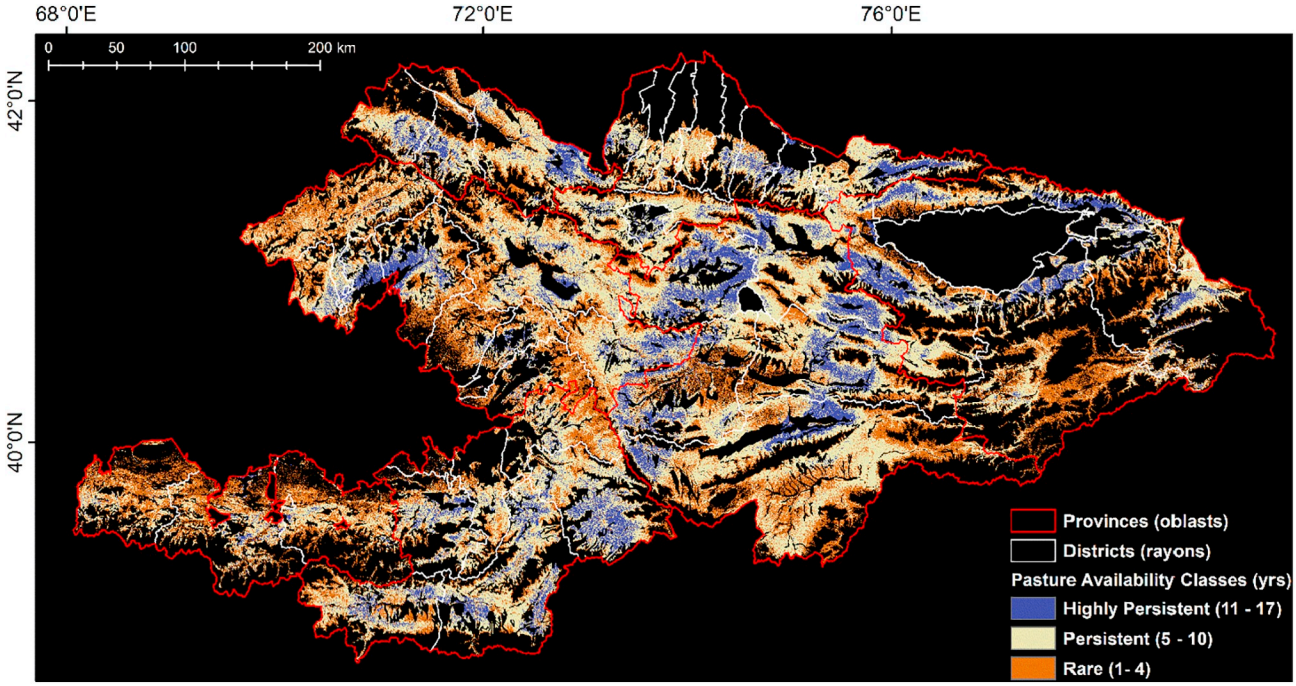

Fig. 8. Pasture Availability classes: Highly Persistent pastures (available during 11–17 years of the 17-year study period) in dark purple; Persistent pastures (5–10 years) in light yellow; and Rarely Available pastures (1–4 years) in orange. Map displays data only for pasture land use areas (Projected coordinate system: Albers Conic Equal Area). (For interpretation of the references to color in this figure legend, the reader is referred to the web version of this article.)

Table 3
Total area in pasture availability class and percentage distribution by elevation class.

Elevation class (m)	Pasture area (km^2)	Highly persistent (%)	Persistent (%)	Rarely available (%)	No fit (%)
< 1800	23,593	16.0	15.5	21.8	28.1
1800–2400	25,487	27.2	25.0	18.9	7.0
2400–2900	21,597	32.9	21.2	13.2	3.4
2900–3400	27,221	21.7	26.8	22.1	9.7
3400–4000	22,038	2.2	11.5	23.6	39.3
> 4000	2469	< 0.01	< 0.1	0.4	12.5
Total	122,405	100.0	100.0	100.0	100.0

41% in P (Table 3).

We calculated averages (over 17 years) for the four phenometrics (PH, TTP, AUC, HTV) derived from the successful fits over the pasture land use areas. Fig. 9 displays maps of the mean values of PH and TTP. Note that the diagonal purple strips apparent in Fig. 8 are not evident in Fig. 9: the former shows frequency and the latter shows average fitted values. Higher PH values (in green) occur at higher elevations over western, northern, and central parts of Kyrgyzstan; whereas, lower PH (in brown) occurs in the central lowlands and over the drier higher elevations in southern Kyrgyzstan. West of Issyk-Kul PH values are low, while they are higher east of the lake. The pattern for TTP is different. In the west near the Ferghana Valley at lower elevations, the TTP mean values are high (in red), and TTP decreases as elevation increases. Over the lowlands in central Kyrgyzstan, where PH is low, TTP is high, and conversely, TTP is low where PH is high. The spatial pattern of mean HTV values closely tracks PH (data not shown).

Mean TTP more closely follows an elevational gradient compared to PH, since air temperature and moisture exhibit lapse rates as a function of altitude, and land surface temperature is related to—but distinct from—air temperature. In contrast, since PH and AUC are driven by abiotic factors (climate, terrain, recent weather), biotic influences (vegetation community, grazing pressure, unpalatable species), and disturbance history (time since landslide, time since grazing, time since drought), they can interact with elevation in complicated ways. Fig. A5, available in the supplemental online material, shows mean AUC values over the 17 years. Over western Kyrgyzstan, where PH and TTP values are high, AUC is also high (dark green). In contrast, over areas where PH is high but TTP is low in the northern highlands, AUC values are lower. However, in the central highlands, where PH is high but TTP is low, mean AUC reaches high values. The lowest AUC values occur at the dry higher elevations in southern Kyrgyzstan.

6.3. Linkages between snow cover and land surface phenology

6.3.1. Correlations among snow cover temporal metrics

We evaluated the relationships among the snow cover temporal metrics by calculating the areas with significant Spearman correlations. Although both SCD and DoSS are related to FDoS and LDoS, the metrics show different relationships. SCD shows the strongest positive connection with DoSS over 53% of both HP area and P areas at $p < 0.05$, and over 31% of both areas at $p < 0.01$ (Table 4). The significant positive correlation of SCD with LDoS occurs over a greater area at $p < 0.05$ (HP: 38%, P: 36%) than the significant negative correlation of SCD with FDoS (HP: 29%, P: 31%). Note that the negative correlation of SCD with FDoS means earlier onset of snow cover that corresponds to higher values of SCD, and the positive correlation of SCD with LDoS means later snowmelt, which also may lead to higher SCD values. In contrast with SCD, > 90% of HP and P areas show a significant negative correlation between DoSS and FDoS at both p-values. The area of significant positive correlation between DoSS and LDoS is just one-third at $p < 0.01$ and over 50% at $p < 0.05$ for HP and slightly lower for P pasture areas (Table 4). FDoS exhibits no significant correlation with LDoS (data not shown). Note that the areas of significant positive correlation between SCD and DoSS are nearly identical for HP and P pasture areas. Similar areal coverages over different pasture classes indicate no or, at most, very weak association between pasture availability classes and relationships among the snow cover metrics.

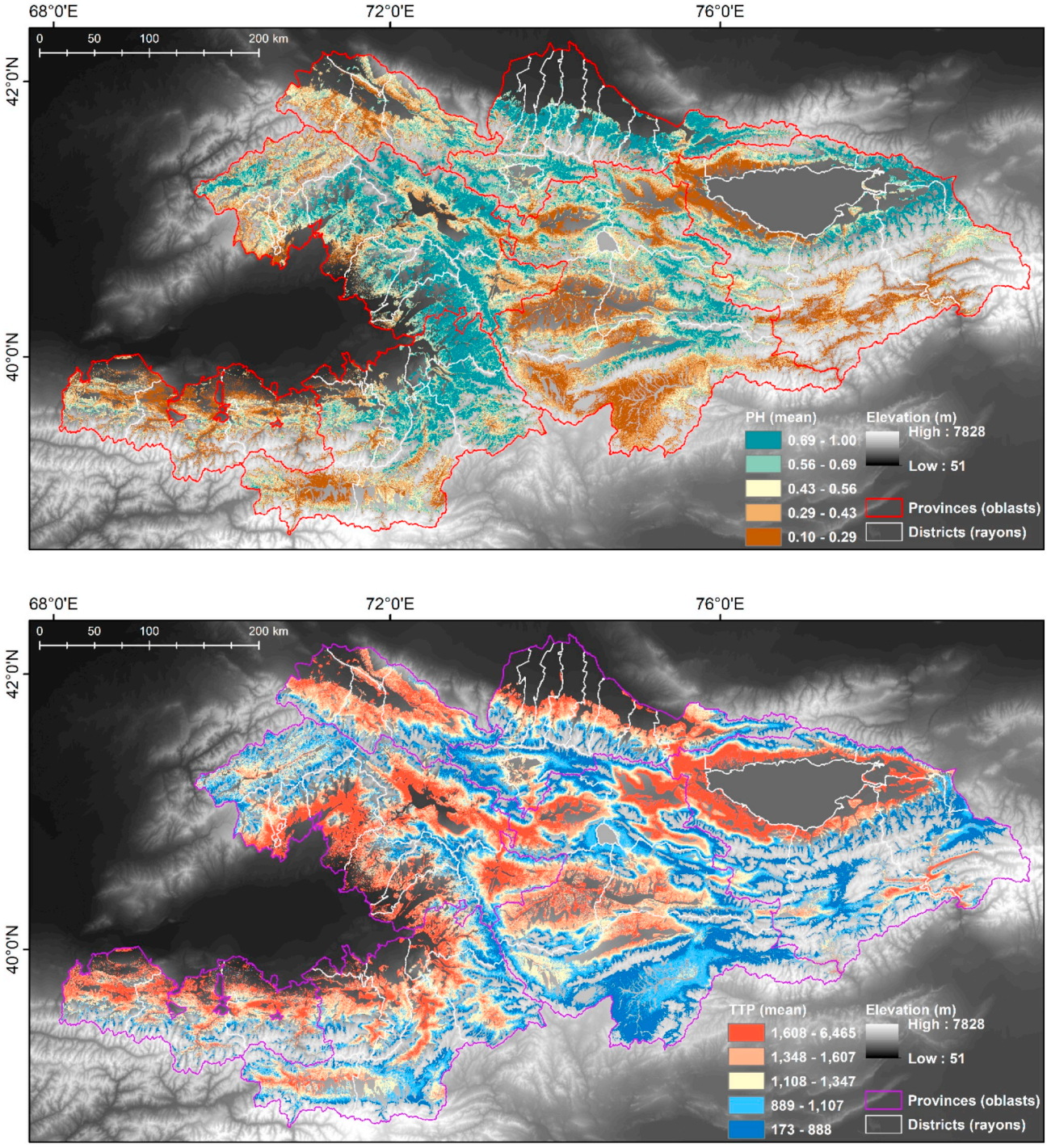

Fig. 9. (Upper) Mean values of Peak Height (PH), (Bottom) Mean values of Time To Peak (TTP). Maps draped over the SRTM 30 m DEM display data only for pasture land use (Projected coordinate system: Albers Conic Equal Area). Classes based on quintiles.

6.3.2. Correlations between snow cover metrics and phenometrics

We also used Spearman correlations to explore the relationships between snow cover temporal metrics and phenometrics. Across the 96 correlations (=4 phenometrics × 4 snow cover temporal metrics × 2 pasture availability classes × 3 significance levels), we focus here on three phenometrics—PH, TTP, and AUC—at $p < 0.01$ and $p < 0.05$ (Tables 4–6). Results for the HTV phenometric appear in Table A2.

PH exhibits predominant positive correlations with SCD, LDoS, and DoSS and one predominant negative correlation with FDoS (Table 5). This pattern holds for HP and P pasture areas at both significance levels. However, spatial predominance is strongest in HP at $p < 0.01$ (Table 5) and, in terms of elevation, the greatest asymmetry occurs for the 2900–3400 m class. Over P pasture areas, the greatest asymmetry occurs at 3400–4000 m (Table 5). For both LDoS and DoSS, the greatest asymmetries occur at 3400–4000 m. In contrast, there is almost no difference between positive and negative correlations of PH with LDoS at the lowest elevation class (< 1800 m). The negative relationship with FDoS dominates over the lowest elevation range over both pastures classes and p-values. However, at the highest elevation class (> 4000 m) of P pasture areas, the relationship changes to positive; there are no HP pasture areas in the highest elevation class.

The pattern of asymmetries with the TTP phenometric show

Table 4
Areal percentage of snow cover temporal metrics with significant positive or negative correlations at p-value < 0.01 and p-value < 0.05 for highly persistent (HP) and persistent (P) pastures.

	SCD				DoSS			
	p < 0.01		p < 0.05		p < 0.01		p < 0.05	
	Pos	Neg	Pos	Neg	Pos	Neg	Pos	Neg
HP (11–17 yrs)								
Area = 15,261 km^2								
FDoS	0.01	13.07	0.12	29.31	< 0.01	92.97	< 0.01	97.6
LDoS	18.44	< 0.01	38.49	0.03	33.34	< 0.01	56.66	0.01
DoSS	31.93	< 0.01	53.47	0.01	–	–	–	–
P (5–10 yrs)								
Area = 53,620 km^2								
FDoS	0.01	13.87	0.08	31.06	< 0.01	94.34	< 0.01	98.13
LDoS	16.6	< 0.01	36.22	0.03	30.46	< 0.01	53.22	0.01
DoSS	31.53	< 0.01	53.17	0.02	–	–	–	–

predominant negative correlations with SCD, LDoS, and DoSS, but no strong asymmetries between TTP and FDoS (Table 6). The negative relationship with SCD predominates at the higher elevation belts: 2900–3400 m and 3400–4000 m over both pasture classes and significance levels. The asymmetry of correlations between TTP and LDoS is similar level regardless of elevation at $p < 0.01$, and the greatest at 2400–2900 m at $p < 0.05$. Over P pastures, the greatest asymmetry occurs at 2400–2900 m (Table 6). The strength of correlation asymmetries between DoSS and TTP are comparable across elevation classes. However, at the highest elevation in HP pastures, there were no pixels at $p < 0.01$, and only very few pixels exhibiting a significant negative relationship at $p < 0.05$. In P pastures, the differences of relationship direction even out. Contrary to the relationship between FDoS and PH, there are no predominant asymmetries for TTP and FDoS, with the sole exception of a significant positive relationship at 3400–4000 m in P pasture areas (Table 6).

Among the four phenometrics, the relationships between the snow cover temporal metrics and AUC are the weakest, with modest asymmetries for LDoS and FDoS in HP and only LDoS in P pastures. Therefore, we do not report asymmetries by elevation class, but instead over the total area for each pasture availability class (Table 7). Similarly, we only report results of HTV for the total area of each pasture availability class (Table A2). As expected, the pattern of HTV closely follows PH, but the linkages of HTV with SCD and FDoS exhibit even stronger asymmetries at each combination of pasture availability class and significance level (Table A2).

6.3.3. Influence of terrain on relationships between snow cover seasonality and phenometrics

We conducted eight exact multinomial tests for equivalence for the nine hotspots shown in Fig. A4. Table 8 presents 95% upper bound for d (p,p_0) of five sets of correlations with p-value < 0.05 at nine hotspots. We marked in bold those values below the specified Δ value of 0.025, indicating that H_0 is rejected, thereby leading to the conclusion that there is no evidence of influence by terrain features on the relationship between the snow cover temporal metrics and the phenometrics at that hotspot.

Of the eight equivalence tests, aspect alone and the interaction between aspect and the 5–10° slope class show weaker influence with 13 and 12 instances of equivalence, respectively, out of the possible 45 (= 5 correlations × 9 hotspots). In contrast, the tests for slope alone, the interaction of aspect and the > 30° slope class, and the overall interaction of aspect and slope each show only three out of 45 occasions of equivalence (Table 8). We can conclude, therefore, that within these hotspots, the primary influence of terrain is slope rather than aspect. SCD exhibited equivalence in nearly 20% of the tests. LDoS, in contrast, had just over 8% equivalence, indicating that both are sensitive to terrain features, but LDoS is more sensitive than SCD (Table 8). While both PH and TTP have comparable levels of equivalence (13% and 11%, respectively), a full quarter of the HTV tests concluded with a finding of equivalence, indicating that HTV was much less sensitive to terrain features than PH or TTP (Table 8).

Over all equivalence tests in the nine hotspots, more terrain sensitivity (fewer cases of equivalence) occurs in hotspots 1, 2, 5, and 9 and less terrain sensitivity in hotspots 4, 7, and 8. Yet, these are sensitivities are relative: each hotspot exhibits some degree of terrain sensitivity in the relationships between snow cover temporal metrics and phenometrics.

7. Discussion

In this study, we have sought to understand the impact of a variable and changing climate on land surface phenology in highland pastures, especially the effects of snow cover seasonality as constrained by terrain. Here we revisit the three research questions articulated in the introduction.

7.1. How does snow cover seasonality relates to subsequent land surface phenology in highland pastures?

Both PH and TTP showed strong and prevalent relationships with the snow cover metrics. Positive correlations of PH and SCD covered a greater areal extent than the negative correlations: significant ($p < 0.05$) positive correlations in HP pastures covered 1568 km^2 or 10.3% of total HP pasture area compared to 126 km^2 or 0.8% in significant negative correlations, more than a twelve-fold difference. Similarly, in P pastures significant positive correlations covered 4225 km^2 or 7.9% of total P pasture area *versus* significant negative correlations over 607 km^2 or 1.1%, nearly a seven-fold difference (Tables 5, 9). More days with snow coverage resulted in greater PH in the following growing season, particularly at the higher elevation ranges: 2900–3400 m of HP and 3400–4000 m for P pastures (Tables 4, 8). A greater areal extent exhibited a significant ($p < 0.05$) negative than positive correlations between SCD and TTP: in HP pastures, 1774 km^2 or 11.6% of the total HP pasture areas compared to 73 km^2 or 0.5%, more than a 24-fold difference; and in P pastures, 4434 km^2 or 8.3% of the total P pastures had significant negative correlations *versus* significant positive correlations in 477 km^2 or 0.9%, more than a nine-fold difference (Tables 6, 9). More snow-covered dates translated into fewer growing degree-days accumulated to reach the thermal time to peak NDVI in the subsequent growing season.

Similar relationships occurred with DoSS, but the area of coverage was twice as small (Tables 6, 9), and the major portion occurs over lower elevation ranges: 1800–2400 m and 2400–2900 m. Later snowmelt also positively influences Peak Height and decreases Thermal Time to Peak, especially at higher elevations. A strong negative relationship was also observed of snowmelt timing and Area Under Curve. For PH the relationship with FDoS (snow onset in preceding snow season) was negative: earlier snow cover increases Peak Height (Tables 6, 9), especially at lowest elevations below 1800 m; whereas, above 4000 m the relationship turned to positive in P pastures. This linkage relates to the necessarily positive correlation between the duration of snow cover season and number of snow-covered dates within that season, since SCD ≤ DoSS, and SCD is typically fewer than DoSS. In the case of TTP and FDoS, there were no clear asymmetries since the areal coverages of both positive and negative correlations were similar, except for positive relationships evident only in Persistent pasture areas between 3400 m and 4000 m (Table 6) over Persistent pastures. Early season AUC showed negative asymmetries with earlier snow onset, but only in HP areas (Table 7). In contrast, early season AUC showed negative asymmetries with earlier snowmelt in both HP and P areas (Table 7).

Table 5
Areal percentage of significant correlations between the snow cover temporal metrics and the phenometric PH and the ratio of positive % area to negative % area at six elevation classes: below 1800 m, 1800–2400 m, 2400–2900 m, 2900–3400 m, 3400–4000 m, above 4000 m, and over total area of each pasture class. In bold with grey background, pos %/neg% > 2.0; *in bold italics, pos%/neg%* < 0.5. NaN means "Not a Number" and results from division by zero.

		PH											
		p<0.01			p<0.05			p<0.01			p<0.05		
		HP (11–17 yrs)						P (5–10 yrs)					
		Pos	Neg	Ratio	Pos	Neg	Ratio	Pos	Neg	Ratio	Pos	Neg	Ratio
SCD	< 1800 m	1.56	0.12	**13.07**	6.45	0.62	**10.38**	1.32	0.34	**3.90**	5.00	1.30	**3.86**
	1800–2400 m	2.80	0.33	**8.51**	8.87	1.36	**6.51**	1.60	0.45	**3.53**	5.73	1.69	**3.40**
	2400–2900 m	4.12	0.21	**20.10**	13.27	0.86	**15.47**	2.10	0.37	**5.65**	7.53	1.39	**5.40**
	2900–3400 m	2.80	0.05	**59.37**	10.45	0.29	**35.61**	2.93	0.15	**19.43**	10.00	0.64	**15.75**
	3400–4000 m	2.40	0.06	**37.88**	8.99	0.32	**28.29**	3.53	0.09	**37.88**	12.13	0.38	**32.17**
	> 4000 m	0.00	0.00	NaN	0.00	0.00	NaN	0.72	0.56	1.30	2.87	2.18	1.32
	TOTAL	3.03	0.19	**15.95**	10.27	0.82	**12.52**	2.24	0.30	**7.47**	7.88	1.13	**6.97**
LDoS	< 1800 m	0.46	0.44	1.03	2.28	2.13	1.07	0.62	0.66	0.95	2.40	2.42	0.99
	1800–2400 m	1.20	0.31	**3.91**	4.89	1.45	**3.37**	0.96	0.56	1.72	3.65	2.12	1.72
	2400–2900 m	2.37	0.16	**15.20**	7.62	0.83	**9.17**	1.49	0.44	**3.41**	5.02	1.72	**2.92**
	2900–3400 m	1.29	0.16	**8.19**	5.00	0.85	**5.90**	1.84	0.27	**6.71**	6.16	1.19	**5.18**
	3400–4000 m	2.24	0.15	**15.41**	8.32	0.71	**11.70**	1.61	0.19	**8.45**	5.93	0.86	**6.87**
	> 4000 m	2.07	0.00	NaN	5.52	0.00	NaN	0.58	0.18	**3.26**	3.70	1.27	**2.90**
	TOTAL	1.51	0.24	**6.29**	5.47	1.21	**4.52**	1.33	0.43	**3.09**	4.68	1.69	**2.77**
DoSS	< 1800m	1.49	0.18	**8.36**	5.90	0.91	**6.51**	1.26	0.44	**2.88**	4.68	1.70	**2.76**
	1800–2400 m	1.67	0.27	**6.18**	6.24	1.28	**4.89**	1.14	0.48	**2.37**	4.34	1.91	**2.27**
	2400–2900 m	1.63	0.22	**7.25**	6.17	1.10	**5.60**	1.21	0.47	**2.57**	4.48	1.93	**2.32**
	2900–3400 m	1.51	0.29	**5.18**	5.64	1.39	**4.07**	1.50	0.42	**3.57**	5.36	1.76	**3.04**
	3400–4000 m	1.66	0.17	**9.96**	6.43	0.86	**7.46**	1.45	0.40	**3.59**	5.26	1.60	**3.29**
	> 4000 m	0.00	0.00	NaN	0.00	1.38	***<0.01***	0.86	0.52	1.64	3.86	2.02	1.90
	TOTAL	1.59	0.24	**6.63**	6.04	1.17	**5.16**	1.31	0.45	**2.91**	4.80	1.81	**2.65**
FDoS	< 1800 m	0.14	2.48	***0.06***	0.71	8.51	***0.08***	0.39	1.87	***0.21***	1.42	6.24	***0.23***
	1800–2400 m	0.28	1.48	***0.19***	1.23	5.62	***0.22***	0.45	1.28	***0.35***	1.72	4.68	***0.37***
	2400–2900 m	0.33	1.04	***0.32***	1.51	4.44	***0.34***	0.54	1.02	0.53	2.12	3.90	0.54
	2900–3400 m	0.46	1.06	***0.43***	2.11	4.01	0.53	0.61	0.94	0.65	2.37	3.50	0.68
	3400–4000 m	0.24	0.80	***0.30***	1.29	3.42	***0.38***	0.57	0.96	0.59	2.16	3.46	0.62
	> 4000 m	0.00	0.00	NaN	1.38	0.00	NaN	0.80	0.31	**2.61**	3.16	1.48	**2.14**
	TOTAL	0.31	1.39	***0.22***	1.43	5.30	***0.27***	0.52	1.19	***0.44***	1.98	4.30	***0.46***

7.2. How do these findings relate to other studies concerning the impact of snow cover on phenology?

Most studies have focused specific dates, *e.g.*, the beginning (SOS), end (EOS), and length (LOS) of the growing season. Our approach uses model phenometrics and, thus, is not directly comparable with the other studies, but it is possible to identify correspondences as well as differences among the findings.

In a study on the QTP, Wang et al. (2018) used MODIS 500 m NDVI dataset and combined 500 m MODIS daily snow products with IMS (National Snow and Ice Data Center's Interactive Multisensor Snow and Ice Mapping System). Their results varied strongly by region, biome, and thermal and moisture regime, but their results are presented in a way that allows for comparison with our results. In the eastern QTP, snow cover duration (number of days with snow cover occurrence within a hydrological year defined in Wang et al. (2018) as the period from 1 September to 31 August of the following year) that corresponds to our SCD, showed a positive correlation with start of growing season (SOS), but it was negatively correlated with length of growing season (LOS), suggesting that longer snow cover delays the spring onset date,

Table 6
Areal percentage of significant correlations between the snow cover temporal metrics and the phenometric TTP and the ratio of positive % area to negative % area at six elevation classes: below 1800 m, 1800–2400 m, 2400–2900 m, 2900–3400 m, 3400–4000 m, above 4000 m, and over total area of each pasture class. In bold with grey background, pos %/neg% > 2.0; *in bold italics, pos%/neg%* < 0.50. NaN means "Not a Number" and results from division by zero.

		TTP											
		p<0.01			p<0.05			p<0.01			p<0.05		
		HP (11–17 yrs)						P (5–10 yrs)					
		Pos	Neg	Ratio	Pos	Neg	Ratio	Pos	Neg	Ratio	Pos	Neg	Ratio
SCD	< 1800 m	0.19	0.90	***0.21***	1.01	4.02	***0.25***	0.37	1.18	***0.32***	1.49	4.43	***0.34***
	1800–2400 m	0.15	2.05	***0.07***	0.84	7.32	***0.11***	0.25	1.57	***0.16***	1.05	5.77	***0.18***
	2400–2900 m	0.03	4.18	***0.01***	0.21	14.06	***0.01***	0.21	2.08	***0.10***	0.87	7.61	***0.11***
	2900–3400 m	0.01	6.50	***<0.01***	0.07	18.23	***<0.01***	0.15	3.49	***0.04***	0.58	11.52	***0.05***
	3400–4000 m	0.02	7.11	***<0.01***	0.12	18.92	***0.01***	0.12	3.85	***0.03***	0.48	12.51	***0.04***
	> 4000 m	0.00	4.14	***<0.01***	0.00	13.79	***<0.01***	0.25	2.04	***0.12***	0.88	6.84	***0.13***
	TOTAL	0.08	3.64	***0.02***	0.48	11.63	***0.04***	0.22	2.40	***0.09***	0.89	8.27	***0.11***
LDoS	< 1800 m	0.13	2.88	***0.04***	0.65	9.71	***0.07***	0.31	1.93	***0.16***	1.14	6.62	***0.17***
	1800–2400 m	0.10	3.18	***0.03***	0.57	10.03	***0.06***	0.26	2.00	***0.13***	1.03	6.85	***0.15***
	2400–2900 m	0.06	3.23	***0.02***	0.36	10.62	***0.03***	0.21	2.22	***0.10***	0.85	7.60	***0.11***
	2900–3400 m	0.11	2.65	***0.04***	0.62	8.71	***0.07***	0.25	2.16	***0.12***	1.01	7.35	***0.14***
	3400–4000 m	0.28	0.96	***0.29***	1.25	4.05	***0.31***	0.37	1.48	***0.25***	1.45	5.05	***0.29***
	> 4000 m	0.00	2.07	***<0.01***	1.38	7.59	***0.18***	0.26	0.59	***0.44***	1.36	3.60	***0.38***
	TOTAL	0.10	2.99	***0.03***	0.54	9.76	***0.06***	0.27	2.02	***0.13***	1.05	6.90	***0.15***
DoSS	< 1800 m	0.24	1.32	***0.18***	1.21	5.02	***0.24***	0.46	1.22	***0.38***	1.80	4.55	***0.40***
	1800–2400 m	0.23	1.37	***0.17***	1.17	5.26	***0.22***	0.39	1.39	***0.28***	1.60	5.08	***0.31***
	2400–2900 m	0.22	1.49	***0.15***	1.09	5.63	***0.19***	0.38	1.45	***0.26***	1.55	5.27	***0.29***
	2900–3400 m	0.19	1.56	***0.12***	0.94	5.93	***0.16***	0.34	1.69	***0.20***	1.42	6.12	***0.23***
	3400–4000 m	0.22	0.91	***0.24***	1.16	3.92	***0.29***	0.40	1.37	***0.29***	1.60	5.02	***0.32***
	> 4000 m	0.00	1.38	***<0.01***	0.00	12.41	***<0.01***	0.80	0.66	1.20	3.20	2.77	1.16
	TOTAL	0.22	1.43	***0.15***	1.10	5.46	***0.20***	0.39	1.45	***0.27***	1.57	5.31	***0.30***
FDoS	< 1800 m	0.58	0.59	0.98	2.40	2.72	0.88	0.73	0.74	0.98	2.73	2.72	1.00
	1800–2400 m	0.60	0.50	1.21	2.63	2.16	1.22	0.84	0.60	1.41	3.14	2.32	1.35
	2400–2900 m	0.74	0.52	1.42	3.19	2.27	1.40	0.95	0.58	1.63	3.53	2.28	1.55
	2900–3400 m	0.78	0.55	1.42	3.34	2.29	1.46	1.14	0.59	1.95	4.14	2.17	1.91
	3400–4000 m	0.57	0.33	1.77	2.67	1.58	1.69	1.06	0.49	**2.14**	3.88	1.85	**2.10**
	> 4000 m	0.69	0.00	NaN	6.90	0.00	NaN	0.49	0.87	0.57	2.11	3.16	0.67
	TOTAL	0.68	0.53	1.28	2.93	2.30	1.27	0.95	0.60	1.58	3.51	2.28	1.54

thereby reducing the duration of the growing season in this very high elevation environment.

In our study, TTP served to indicate the length of green-up period, and we found a substantially greater area of negative than positive relationship of TTP with the number of snow-covered dates over the study area. Wang et al. (2018) concluded, counterintuitively, that longer snow cover duration led to an earlier SOS and longer growing season.

In terms of the snow cover melting dates, they detected two opposed relationships with SOS: a positive correlation between snow cover melting date and SOS occurred in most areas—except alpine steppe—but a negative correlation appeared over warmer, drier areas where snow melted too early for the vegetation to take advantage of the meltwater (Wang et al., 2018). Snow cover melting date was positively correlated with LOS in the eastern and southwestern part of QTP, while negative correlations were observed over much of the central Plateau. If we consider our LDoS metric as functionally equivalent to their snow cover melting date, a predominantly negative relationship between LDoS and TTP was also evident in our results. Finally, they found the maximum NDVI showed positive correlation with snow cover duration and snow cover melt date, which are findings similar to ours: where we found that PH was been positively correlated with SCD, DoSS, and

Table 7
Areal percentage of significant correlations between the snow cover temporal metrics and the phenometric AUC and the ratio of positive % area to negative % area. In bold, pos%/neg% > 2.0; *in bold italics, pos%/neg% < 0.5.*

	AUC					
	p < 0.01			p < 0.05		
	Pos	Neg	Ratio	Pos	Neg	Ratio
HP (11–17 yrs) Area = 15,261 km^2						
SCD	0.32	0.52	0.62	1.75	2.42	0.72
LDoS	0.28	1.04	***0.27***	1.35	4.45	***0.30***
DoSS	0.56	0.51	1.10	2.58	2.33	1.11
FDoS	0.31	0.87	***0.36***	1.52	3.80	***0.40***
P (5–10 yrs) Area = 53,620 km^2						
SCD	0.57	0.66	0.86	2.29	2.56	0.89
LDoS	0.42	1.05	***0.40***	1.67	4.00	***0.42***
DoSS	0.60	0.78	0.77	2.39	3.09	0.77
FDoS	0.64	0.80	0.80	2.46	3.06	0.80

LDoS, and negatively correlated with FDoS, meaning that when snow occurred earlier and lasted longer on the ground, the NDVI was higher in the subsequent growing season.

Qiao and Wang (2019) explored relationships between winter snow cover dynamics, climate and spring grassland vegetation phenology in Inner Mongolia, China using AVHRR-NDVI dataset at ~5 km spatial resolution and meteorological station data for precipitation and temperature.

In general, Qiao and Wang (2019) found positive relationships of the start of the growing season with snow cover duration and with snow cover melt date.

We found a negative relationship between FDoS and PH, meaning earlier FDoS positively influenced PH, and Qiao and Wang (2019) found a negative relationship between snow cover onset date and the start of the growing season. Variable influence of snow cover depth on SOS was reported by Yu et al. (2013) in the study over China, where increasing snow depth could either advance or delay the SOS, depending on elevation, vegetation type, and climatic zone.

Paudel and Andersen (2013) explored responses of rangeland vegetation to snow cover dynamics in Nepal Trans Himalayas using MODIS NDVI data at 250 m and MODIS snow cover product at 500 m

Table 8
Results of exact multinomial tests for equivalence: values of 95% upper bound for $d(p,p_0)$. In bold are values below $\Delta = 0.025$, meaning H_o is rejected and we conclude equivalence and no significant terrain effect. Note in hotspot 9, the significant negative correlation between PH and LDoS *is highlighted in italics.* In every other hotspot, the significant correlation between PH and LDoS was positive.

Dataset	Hotspot	Aspect	Slope	0–5° × aspect	5–10° × aspect	10–15° × aspect	15–30° × aspect	> 30° × Aspect	Slope × aspect
PH SCD pos	HS1	0.025	**0.021**	0.033	**0.021**	0.050	0.047	0.064	**0.022**
PH LDoS pos		0.025	0.091	0.058	0.031	0.045	0.039	0.050	0.091
TTP SCD neg		0.055	0.096	0.027	0.062	0.080	0.058	0.043	0.096
TTP LDoS neg		0.030	0.087	0.029	0.032	0.042	0.037	0.048	0.092
HTV SCD pos		0.050	0.053	**0.016**	0.040	0.077	0.083	0.087	0.053
PH SCD pos	HS2	0.037	0.100	0.043	**0.025**	0.027	0.054	0.051	0.101
PH LDoS pos		**0.024**	0.053	0.042	0.033	0.033	0.032	0.043	0.056
TTP SCD neg		**0.023**	0.084	0.045	0.051	0.050	0.042	0.070	0.086
TTP LDoS neg		0.026	0.080	0.028	0.058	0.046	0.052	0.052	0.080
HTV SCD pos		0.043	0.104	0.055	0.041	0.044	0.060	0.063	0.107
PH SCD pos	HS3	**0.014**	0.038	**0.023**	**0.018**	**0.013**	0.026	0.032	0.040
PH LDoS pos		0.037	0.100	0.034	0.046	0.030	**0.020**	0.066	0.102
TTP SCD neg		0.035	0.089	0.033	0.035	0.079	0.064	0.096	0.094
TTP LDoS neg		0.041	0.184	0.036	0.051	0.057	0.027	0.042	0.184
HTV SCD pos		0.028	0.034	0.027	0.031	0.033	0.042	0.038	0.038
PH SCD pos	HS4	**0.017**	0.028	**0.007**	**0.016**	0.032	0.028	0.032	0.030
PH LDoS pos		0.045	0.050	**0.023**	0.034	0.050	0.072	0.100	0.050
TTP SCD neg		0.027	0.067	**0.021**	0.043	0.070	0.057	0.045	0.069
TTP LDoS neg		0.050	0.128	0.025	0.085	0.109	0.083	0.132	0.132
HTV SCD pos		**0.009**	0.066	**0.009**	**0.016**	**0.019**	**0.023**	0.049	0.066
PH SCD pos	HS5	0.028	0.067	0.050	0.034	**0.020**	0.032	0.047	0.067
PH LDoS pos		0.031	0.033	0.044	**0.024**	0.045	0.027	0.060	0.033
TTP SCD neg		**0.020**	0.025	0.036	0.028	0.052	0.040	0.085	0.025
TTP LDoS neg		0.040	0.099	0.082	0.037	0.050	0.035	0.087	0.105
HTV SCD pos		0.055	0.044	0.039	**0.025**	0.043	0.087	0.088	0.044
PH SCD pos	HS6	0.056	0.083	0.058	0.059	0.075	0.053	0.059	0.084
PH LDoS pos		0.031	0.076	0.044	0.044	0.031	0.034	0.041	0.076
TTP SCD neg		0.026	0.083	**0.022**	**0.024**	**0.018**	0.029	0.037	0.083
TTP LDoS neg		0.046	0.096	**0.021**	**0.024**	0.025	0.052	0.056	0.106
HTV SCD pos		0.055	0.043	0.049	0.050	0.059	0.068	0.055	0.061
PH SCD pos	HS7	0.031	0.029	0.052	0.040	0.045	0.039	0.029	0.030
PH LDoS pos		**0.021**	0.106	0.038	**0.020**	0.029	0.028	0.056	0.106
TTP SCD neg		**0.022**	0.115	0.044	0.038	0.039	**0.022**	0.033	0.117
TTP LDoS neg		0.032	**0.015**	0.032	0.034	0.042	0.035	0.043	0.027
HTV SCD pos		**0.016**	**0.020**	0.069	0.041	0.026	**0.018**	**0.022**	**0.022**
PH SCD pos	HS8	**0.019**	0.078	0.033	0.066	0.048	0.047	**0.020**	0.078
PH LDoS pos		0.040	0.052	0.095	0.087	0.050	0.036	0.035	0.061
TTP SCD neg		**0.015**	0.026	0.068	**0.017**	**0.022**	**0.023**	0.049	0.031
TTP LDoS neg		**0.024**	0.040	0.078	0.031	**0.020**	0.027	0.042	0.040
HTV SCD pos		**0.017**	0.072	0.051	0.051	**0.023**	**0.008**	**0.024**	0.072
PH SCD pos	HS9	0.041	0.046	0.051	0.037	0.036	0.045	0.065	0.050
PH LDoS neg		0.033	0.036	0.036	0.026	0.035	0.047	0.057	0.038
TTP SCD neg		0.059	0.091	0.050	0.054	0.058	0.062	0.129	0.094
TTP LDoS neg		0.026	0.060	0.026	**0.018**	0.026	0.033	0.041	0.060
HTV SCD pos		0.052	0.098	0.045	0.036	0.038	0.054	0.094	0.100

Table 9
Areal extent (km^2) of significant correlations between metrics of snow cover seasonality and phenometrics from the following growing season. TTP is Thermal Time to Peak; PH is Peak Height; SCD is Snow-Covered Dates; LDoS is Last Date of Snow cover; DoSS is Duration of Snow Season; FDoS is First Date of Snow cover; HP indicates highly persistent and P indicates persistent pasture areas. Positive correlations on grey background; negative correlations on white background.

		TTP				PH			
		p<0.01		p<0.05		p<0.01		p<0.05	
		HP	P	HP	P	HP	P	HP	P
SCD	< 1800m	22	99	99	368	38	110	158	416
	1800–2400m	85	211	304	774	116	215	368	769
	2400–2900m	210	236	706	861	207	238	666	852
	2900–3400m	215	501	603	1,656	93	422	346	1,437
	3400–4000m	24	238	63	773	8	218	30	750
	> 4000m	<0.01	<0.5	<0.01	2	–	<0.5	–	<1
	TOTAL	556	1,284	1,774	4,434	462	1,202	1,568	4,225
LDoS	< 1800m	71	161	238	550	11	52	56	200
	1800–2400m	132	268	416	919	50	128	203	489
	2400–2900m	162	251	533	860	119	168	383	568
	2900–3400m	88	310	288	1,056	43	265	166	885
	3400–4000m	3	91	13	312	7	100	27	366
	> 4000m	<0.01	<0.5	<0.01	1	<0.01	<0.5	<0.01	<1
	TOTAL	456	1,082	1,489	3,699	230	713	835	2,508
DoSS	< 1800m	32	101	123	378	37	105	145	389
	1800–2400m	57	186	218	681	69	153	259	582
	2400–2900m	75	164	283	596	82	136	310	507
	2900–3400m	52	243	196	880	50	216	187	770
	3400–4000m	3	85	13	310	5	90	21	325
	> 4000m	<0.01	<0.5	<0.5	1	0	<0.5	0	<1
	TOTAL	219	779	833	2,847	243	700	921	2,574
FDoS	< 1800m	14	61	59	227	61	156	209	518
	1800–2400m	25	113	109	421	61	172	233	628
	2400–2900m	37	107	160	400	52	115	223	442
	2900–3400m	26	164	111	594	35	135	133	504
	3400–4000m	2	65	9	240	3	59	11	214
	> 4000m	<0.01	<0.5	<0.01	<0.5	0	<0.1	0	<0.5
	TOTAL	104	510	447	1,883	212	637	809	2,306

resolution over the 2000–2009 period. They observed significant positive correlations between SOS and the last snow-free date in drier areas at higher elevations (above 4000 m), while negative or no significant correlations were observed at lower elevations (3000–4000 m). To evaluate the relationship between snow cover duration and vegetation production in different ecozones, they used pre-monsoon NDVI time-integrated from April to June over four different sites and in four elevational belts (< 3000 m, 3000–4000 m, 4000–4500 m, and > 4500 m), while we used an early season AUC metric, which could be considered comparable to their time-integrated NDVI. They observed strong positive relationships between snow cover duration and the time-integrated NDVI at the driest location over elevation above 3000 m, and the strengthening of that relationship toward higher elevation ($p < 0.01$). In contrast, there was a negative linear relationship at the wetter site in every elevation class ($p < 0.05$).

The significant influence of elevation on relationship strength observed by Paudel and Andersen (2013) points to strong terrain effects (and related thermal-moisture conditions) on snow cover-vegetation relationships, which we found in our study (*cf.* Section 6.3.3). If we consider our early season AUC metric to be related to their time-integrated NDVI, we found the correlations with the snow cover metrics to be the weakest in terms of areal extent among the four phenometrics. Moreover, only three correlations exhibited substantial asymmetries, where the ratio of areal extent of positive to negative correlations was lower than our threshold of 0.5 meaning a much greater area of significant negative correlations (*cf.* Section 6.3.2). This situation appeared in HP pastures for correlations between AUC and LDoS and AUC and FDoS, but in P pastures only between AUC with LDoS (Table 7).

Paudel and Andersen (2013) observed a strong negative relationship of time-integrated NDVI and snow cover duration over rather relatively

wetter areas of study sites, but positive over drier regions. In contrast, we found a slightly greater area of the negative correlation between AUC and SCD (*pos%/neg%* = 0.62 for HP and 0.86 for P pastures at $p < 0.01$). However, as those asymmetries did not cross our threshold of 0.5, the distributions were deemed not to be substantially different. Further, we integrated NDVI by GDD only up to the fitted PH, thus affecting linkages with the snow cover metrics. Furthermore, the interannual variation of AUC may also have been affected by local factors such as grazing and pasture management practices and disturbance history (*e.g.*, landslides and mudflows). Finally, the threshold values for AGDD (100) and NDVI (0.1) we used for the AUC calculation may have affected the strength of the relationships.

Overall, our study and the others all agreed on the strong influence of snow cover on shaping growing season dynamics, although the patterns differed due to elevation, vegetation community, and climatic characteristics.

7.3. How does mountainous terrain modulate snow cover effects?

Highland pasture phenology depends on the thermal regime of growing season. Over mountains, the growing season is shaped by terrain features. Elevation, aspect, and slope all play crucial roles (An et al., 2018), and can have strong effects on vegetation species richness, productivity, and nutrient dynamics (Gong et al., 2008).

In our study, the longest warm season (Fig. 6; $AGDD_{max}$ in Table 2) occurred in the lowest elevation class (below 1800 m) showing similar low variability over the years, while with the increasing elevation, the warm season length ($AGDD_{max}$, Table 2) decreased and interannual variation increased, especially during summer time (Fig. 6). However, when we divided the data into contrasting aspects (Fig. 7), we found greater differences in the length of thermal time on northern aspects than in southern aspects, which might arise from higher variation in soil moisture on steeper slopes. The soil moisture-slope-aspect interaction influences species composition and productivity due to water availability (Armesto and Martinez, 1978; Badano et al., 2005; Måren et al., 2015; Sternberg and Shoshany, 2001). Change in the length of the warm season is strongly influenced by elevation. The difference between warm seasons on different slopes increased at higher elevations and became more significant and more pronounced on steeper slopes (Fig. 7). Erosion processes may limit vegetation growth and development on steeper slopes. In addition, soil weathering can be accelerated on south-facing slopes resulting in different soil properties (*e.g.*, changes in organic soil layer) in northern *versus* southern aspects (Gong et al., 2008; Xue et al., 2018). The aspect of the slope can lead to local environmental conditions unfavorable for plant growth, *e.g.*, where sun exposure might be longer over southern aspects leading to the lower soil moisture and soil nutrient levels. In the recent study in alpine meadows on the QTP, Liu et al. (2019) observed that plant leaves have better growing conditions, the higher moisture content, and the lower dry matter content in the leaves over northern aspects due to higher soil moisture and soil nutrient levels (Sternberg and Shoshany, 2001). On the other hand, the edaphic factors on southern aspects could help to maintain more stress-tolerant and light-demanding flora (Bennie et al., 2006; Liu et al., 2019).

Findings of An et al. (2018) indicate that in complex terrain at high elevation, the temperature-moisture combinations strongly shapes the land surface phenology with slope playing a key role in the vegetation development. Those results are in correspondence with our findings. Results from the exact multinomial tests for equivalence (Table 8) point to the predominant role of slope in shaping interactions between snow seasonality metrics and phenometrics. Slope alone, the interaction of aspect with the > 30° slope class, and the overall interaction of slope and aspect all show the lowest number of equivalence occurrences (just three null hypotheses rejected out 45 tests). In contrast, aspect alone had 29% (13/45) of null hypotheses rejected. Moreover, relationships with LDoS show fewer conclusions of equivalence overall than relationships with SCD (11 *vs.* 41, Table 8), which may indicate a more sensitive relationship between the timing of the end of snow season and subsequent phenology over complex terrain, and the higher instability of LDoS (*cf.* Section 7.3). Terrain complexity affects the relationship between snow seasonality and pasture phenology. In general, longer snow cover favors higher peak height, but terrain features—especially elevation—can modify that relationship.

Results of the Xie et al. (2017) showed the role of snow cover greatly varies due to elevation, vegetation type, and climate. When considering the influence of elevation, they found that the correlations between duration and LSP varied over low elevation (< 1000 m) and mid-elevation (1000–2000 m), while with increasing elevation they weaken and eventually disappear toward the highest elevations. < 10% of their study sites showed a weak correlation between last snow day and LSP metrics. In contrast, we found different results in our study: the strength of significant correlation asymmetries between snow cover temporal metrics and LSP generally increased with elevation. Also, a greater area of those relationships were reported at higher elevation ranges (Tables 5, 6, 9). This finding indicates a higher sensitivity of vegetation to changes in weather patterns at higher elevations. The exception was the relationship between FDoS and PH, where the area of negative relationship decreased with increasing elevation and became positive relationship above 4000 m, although the areal extent was very small (*cf.* Section 6.3.2, Table 5).

Terrain effects and elevational gradients may differentially affect vegetation productivity and susceptibility to disturbance. In a study across the Great Basin region in the western United States over Sierra Nevada, Ruby, and Wasatch/Uinta mountain ranges where elevation reaches above 4300 m, Petersky et al. (2019) showed that vegetation types used to have a consistent seasonal snow cover in their historical record were likely to have lower resilience under a new hydrologic regime (longer but drier growing season) resulting from warming trends that generated rain on snow events. However, the implications of the changes in snow cover persistency and vegetation sensitivity varied locally due to elevation and topographic complexity. In addition, those consequences depended on groundwater availability and potential physiological adaptation by the vegetation communities.

7.4. What can recent changes in snow cover seasonality tell us about possible futures for highland pasture phenology and productivity?

Snow cover can experience multiple melting episodes over the snow season in the highland pastures of Kyrgyzstan. Our results show the positive correlation between SCD and DoSS was significant but relatively low: just over 30% of each pasture availability class at $p < 0.01$ and up to 53% at $p < 0.05$. Annual high variation of snow cover duration, especially in southeastern Kyrgyzstan, has also been reported by Dedieu et al. (2014) based on MOD10 snow products.

DoSS showed > 90% of area negatively correlated with FDoS at both significance levels, and only 30% to 50% of positive correlation with LDoS. That higher correlation of DoSS and FDoS than DoSS with LDoS, would suggest a greater dependence of snow cover duration on the snow onset date than on end date. However, the much smaller area of negative correlation between SCD and FDoS, and positive relationship between SCD and LDoS means high variation of snow cover over the season, especially at a beginning of snow cover season when the depth is still small and snowmelt can easily occur. Of the four snow metrics, SCD played a leading role in influencing pasture phenology, and a similar conclusion reached by Xie et al. (2018) in their study of alpine LSP. The negative relationship between TTP and snow metrics

may mean more days for pasture vegetation to grow. The connection of soil moisture and growth rate could also be explained by the large area of positive correlation between of SCD and PH more days with snow cover may add moisture to soil, and have crucial effects on soil heat and moisture preservation due to the insulating properties of the snowpack (Groffman et al., 2001; Qiao and Wang, 2019). HTV, which occurs earlier in the season, follows the correlation patterns of PH, and also shows positive relationships with SCD and DoSS.

The most important consequence of the shifts in the snow cover seasonality for mountainous vegetation is the alteration of the timing and rates of water availability and snow-insulation benefits. Shifts in vegetation structure and composition in response to new thermal and hydrological regimes (Telwala et al., 2013; Xie et al., 2018) in semiarid regions are likely to have cascading implications on large-scale water, carbon budgets, and susceptibility to disturbance (Petersky et al., 2019). Here, we found the strongest response of LSP metrics to changes in snow cover temporal metrics occurred at higher elevations. A study over the Himalayas (Telwala et al., 2013) showed, that over higher elevations the stronger warming-driven range shift of vegetation distribution was evident and vegetation composition richness had been declining. They concluded that the continued trend of warming was likely to result in ongoing shifts in elevational range distributions and, eventually, species extinctions, particularly at mountaintops due to compression of suitable habitat In a study in the French Alps, where mean elevation was about 2600 and ranged between 1000 and 4000 m, Choler (2015) showed that the length of the snow-free period was the primary determinant at productivity in temperate montane grasslands, and later snowmelt dates had a strong negative impact on the grassland productivity. We found a greater area of significant negative than positive correlation between LDoS and AUC, meaning a later snowmelt translated into a lower AUC to PH.

7.5. Limitations, uncertainties, and paths forward

Remote sensing studies of snow effects on vegetation are limited by the relatively short duration of most sensor archives and by the rather coarse spatial resolution of pixels relative to the spatial heterogeneity encountered in mountainous terrain. Within the area of a 500 m pixel it is not possible to state snow spatial distribution or its condition, while the use of higher spatial resolution data (*i.e.*, ≤ 30 m) may deliver more detailed information, especially in terms of the spatial distribution of snow cover. However, the temporal resolution of most sensors does not allow for observations at a tempo to characterize well the changes in a melting snowfield. Thus, while remote sensing datasets may be well suited for landscape scale research, and may be not appropriate for local field studies where the objects of interest are particular species or plant communities. In addition, frequent cloudiness lowers the number of clear observations and generates uncertainty in the differentiation of snow from clouds (Ackerman et al., 2008; Crane and Anderson, 1984). Our use of 8-day snow cover composites may introduce some temporal imprecision into the study, but the use of composites also provides consistent statistical power for trend analyses. In the 8-day composites, the maximum snow extent occurs where snow was observed on at least one day during the 8-day period. Therefore, a pixel may be marked as snow in two consecutive composites, but there might be no actual snow coverage on the land between the beginning of the first period and the end of the second period. This situation may lead to uncertainty in the determination of snow cover duration. However, these products have undergone extensive evaluation and validation, with additional screening in V006, so we concluded it was a suitable product for our study despite its limitations.

Moving forward, the relatively new Theia snow collection is a high-resolution operational snow cover mapping system based on Sentinel-2 and Landsat-8 datasets (Gascoin et al., 2019) at 20 m spatial resolution, may offer new possibilities for snow-vegetation interaction studies at local scales.

Studies of the influence of snow cover on phenology are complicated by local interactions between terrain, vegetation, and microclimate; thus, synergistic analysis with higher spatial resolution image time series from digital cameras (Liu et al., 2017; Melaas et al., 2016; Rossi et al., 2019; Watson et al., 2019; Yan et al., 2019) might also provide a productive avenue for balancing spatial and temporal resolutions (Julitta et al., 2014; Westergaard-Nielsen et al., 2017).

With the advent of the Sentinel-2 datastreams in the late 2010s, the combination with Landsat observations into a harmonized surface reflectance product offers a much richer source of observations for moving forward (Claverie et al., 2018), but does not necessarily produce better characterization of LSPs (Nguyen and Henebry, 2019).

Using our specified conditions for fitting and additional filtering of observations surely reduced the number of available pixels for subsequent analyses. That data reduction potentially introduces additional uncertainties into the analysis of pasture phenologies, *e.g.*, by influencing the shape of the parabola. However, a similar analytical approach has been used successfully in the study of LSP across Central Asia, albeit at a much coarser spatial resolution (de Beurs et al., 2018).

Finally, we did not account for human impacts on pasture phenology that can arise from stocking rates, herd management, pasture maintenance, and control of invasive species, each of which may add to uncertainties that may affect some findings of this study (Eddy et al., 2017; Karnieli et al., 2013; Zhumanova et al., 2016, 2018). However, our study focused primarily on the early season green-up dynamics when differential effects from grazing management are expected to be minimal.

8. Conclusions

We investigated the effects of snow cover timing and duration on the land surface phenology during the following growing season across the highland pastures of Kyrgyzstan. Our results show strong interactions between snow cover timing and metrics of land surface phenology and these interactions differ due to location, elevation, and terrain characteristics. We found a positive relationship between the number of composite dates with snow cover (SCD) and the amplitude of the fitted phenological curve (PH). We also found that later timing of snowmelt (LDoS) also increased the amplitude of the fitted phenological curve. On the other hand, a negative correlation was found between the onset of snow cover (FDoS) and the amplitude of the fitted phenological curve. Relationships of the snow cover temporal metrics with the amount of thermal time needed to reach the peak amplitude of the fitted curve were negative, with the strongest relationship between the number of snow-covered dates (SCD) and the amount of thermal time needed to reach the peak amplitude (TTP).

We further demonstrated that the mountainous terrain affected linkages between snow cover and pasture phenology. The most pronounced effects were on the timing of snowmelt (LDoS) with slope being more influential than aspect, and the strongest interaction being aspect on steeper slopes. Over the highest elevations, the interplay of steep slopes and aspects strongly decreased growing season duration. We also observed a slight increase in areal extent asymmetries of positive and negative correlations between snow cover temporal metrics and LSP toward higher elevations (up to 4000 m).

While this paper has focused on establishing linkages between snow cover seasonality and metrics of land surface phenology in highland pastures, there is a need to zoom out from the landscape to see the broader biospheric context. One direction for future research is to explore how the modes of climate oscillations affect local weather

patterns and, thus, potentially snow cover seasonality and LSP (Alemu and Henebry, 2013; de Beurs et al., 2018; de Beurs and Henebry, 2010b; Gonsamo and Chen, 2016; Pervez and Henebry, 2015; Viña and Henebry, 2005; Wright et al., 2014; Yeo et al., 2017). There is also need to analyze both snow cover seasonality and pasture phenology over particular colder/drier and warmer/wetter years to describe in detail how the phenometrics behave under different weather sequences, and if the behaviors vary due to the terrain features. Eventually, the introduction of additional datasets with higher spatial and temporal resolutions could improve the precision and accuracy of the analyses, especially over the challenging terrain of montane Central Asia.

CRediT authorship contribution statement

Monika A. Tomaszewska: Conceptualization, Data curation, Formal analysis, Investigation, Methodology, Software, Visualization, Writing - original draft, review & editing. **Lan H. Nguyen:**Methodology, Software, Writing - review & editing. **Geoffrey M. Henebry:**Conceptualization, Data curation, Formal analysis, Funding acquisition, Investigation, Methodology, Project administration, Resources, Supervision, Validation, Visualization, Writing - review & editing.

Declaration of competing interest

The authors declare that they have no known competing financial interests or personal relationships that could have appeared to influence the work reported in this paper.

Acknowledgments

This research was supported, in part, by the US NASA Land Cover/Land Use Change Program (NNX15AP81G) *How Environmental Change in Central Asian Highlands Impacts High Elevation Communities*. We appreciate the assistance and feedback from A.A. Aidaraliev, K. Kelgenbaeva, and P. Maatkarimov. We thank J. Frey of Villanova University for sharing his expertise and code that enabled us to run the exact multinomial test for equivalence. We thank the three anonymous reviewers whose helpful comments enabled us to increase the relevance and clarity our research presentation.

Appendix A

A.1. Exploratory analysis of topographic corrections on NDVI data within the study area

We used two Landsat-8 OLI tiles from Collection 1 Tier 1 Level-1 Precision and Terrain (L1TP) corrected product acquired on 07 July 2017 (Path 150 Row 030) and on 30 July 2017 (Path 152 Row 032), to which we applied seven topographic correction methods (Goslee, 2011). There are two families of topographic correction methods. The first is Lambertian method, which assumes that the reflectance of all wavelengths is constant and independent of viewing angle, and for which the correction factor is identical for all bands. In addition, only the direct part of the irradiance is modeled. The second family is composed of the non-Lambertian methods that consider surface roughness, which means the interaction of incident and view angles influences the observed radiance (Riaño et al., 2003).

At two locations where the topography corrections were performed, the results of four Lambertian methods—Cosine, Improved Cosine, Gamma, and Sun-Canopy-Sensor (SCS)—showed that the difference between the NDVI calculated from the original and corrected bands was minimal, regardless of terrain. The higher differences were generated using the three non-Lambertian methods (Minnaert, Minnaert + Slope, and C-Correction), which showed that differences reached up to 4% over the steepest slopes ($> 30^{\circ}$) when the NDVI values were lower (~0.2–0.3). At the peak summer when the Landsat data were collected, NDVI values of 0.2 to 0.3 would indicate sparse vegetation than values typical of pasture at that time of year. We concluded that topographic corrections were unnecessary for our study because the magnitude of the correction to the NDVI was so much smaller than the seasonal NDVI signal. Moreira et al. (2016) also concluded that the NDVI was robust to topographic effects.

Table A1
Landsat tiles for each sensor and year. Paths from 147 to 155, rows from 30 to 33.

	LT5		LE7		LC8		
	Unique	Total	Unique	Total	Unique	Total	
2001	5	18	33	312	–	–	
2002	3	3	33	286	–	–	
2003	0	0	33	273	–	–	
2004	0	0	33	432	–	–	
2005	0	0	33	457	–	–	
2006	11	44	33	451	–	–	
2007	9	54	33	512	–	–	
2008	32	228	32	488	–	–	
2009	33	533	33	455	–	–	
2010	33	451	33	425	–	–	
2011	33	406	33	433	–	–	
2012	0	0	33	581	–	–	
2013	–	–	33	621	33	518	
2014	–	–	33	633	33	685	
2015	–	–	33	643	33	678	
2016	–	–	33	622	33	682	
2017	–	–	33	653	33	708	
TOTAL		1737		8277		3271	13,285

Table A2
Areal percentage of significant correlations between snow cover temporal metrics and the phenometric HTV and the ratio of positive % area to negative % area. In bold, pos%/neg% > 2.0; *in bold italics, pos%/neg%* < 0.5.

	HTV					
	p < 0.01			p < 0.05		
	Pos	Neg	Ratio	Pos	Neg	Ratio
HP (11–17 yrs)						
Area = 15,261 km^2						
SCD	2.87	0.11	**26.09**	10.63	0.51	**20.84**
LDoS	1.36	0.22	**6.18**	5.30	1.12	**4.73**
DoSS	1.71	0.22	**7.77**	6.37	1.07	**5.95**
FDoS	0.27	1.47	***0.18***	1.30	5.60	***0.23***
P (5–10 yrs)						
Area = 53,620 km^2						
SCD	2.45	0.25	**9.80**	8.46	0.97	**8.72**
LDoS	1.25	0.43	**2.91**	4.38	1.76	**2.49**
DoSS	1.40	0.42	**3.33**	5.05	1.71	**2.95**
FDoS	0.47	1.30	***0.36***	1.81	4.65	***0.39***

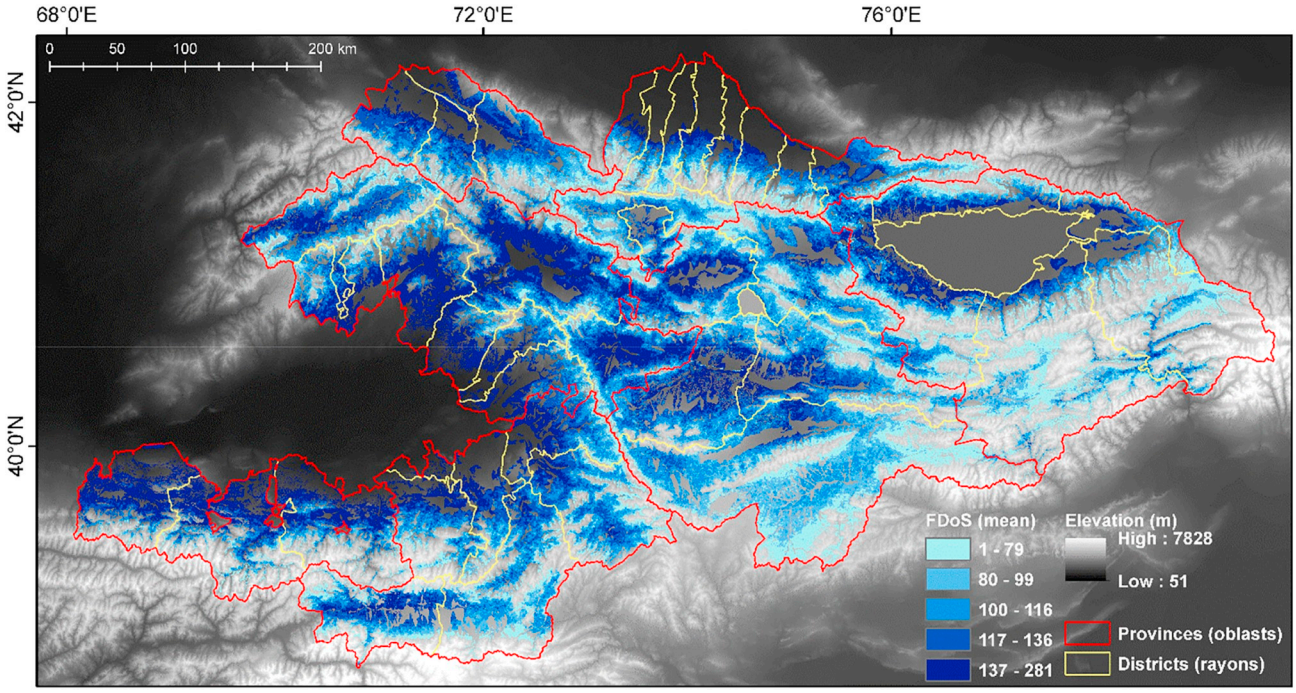

Fig. A1. Mean values of First Day of Snow (FDoS). Note that those values refer to the snow season range from 1 to 361 using MODIS 8-day composites. Thus, value 1 is equivalent to $DOY169_{year}$ using the MODIS 8-day composites naming convention. Map draped over the SRTM 30 m DEM display data only for pasture land use (Projected coordinate system: Albers Conic Equal Area).

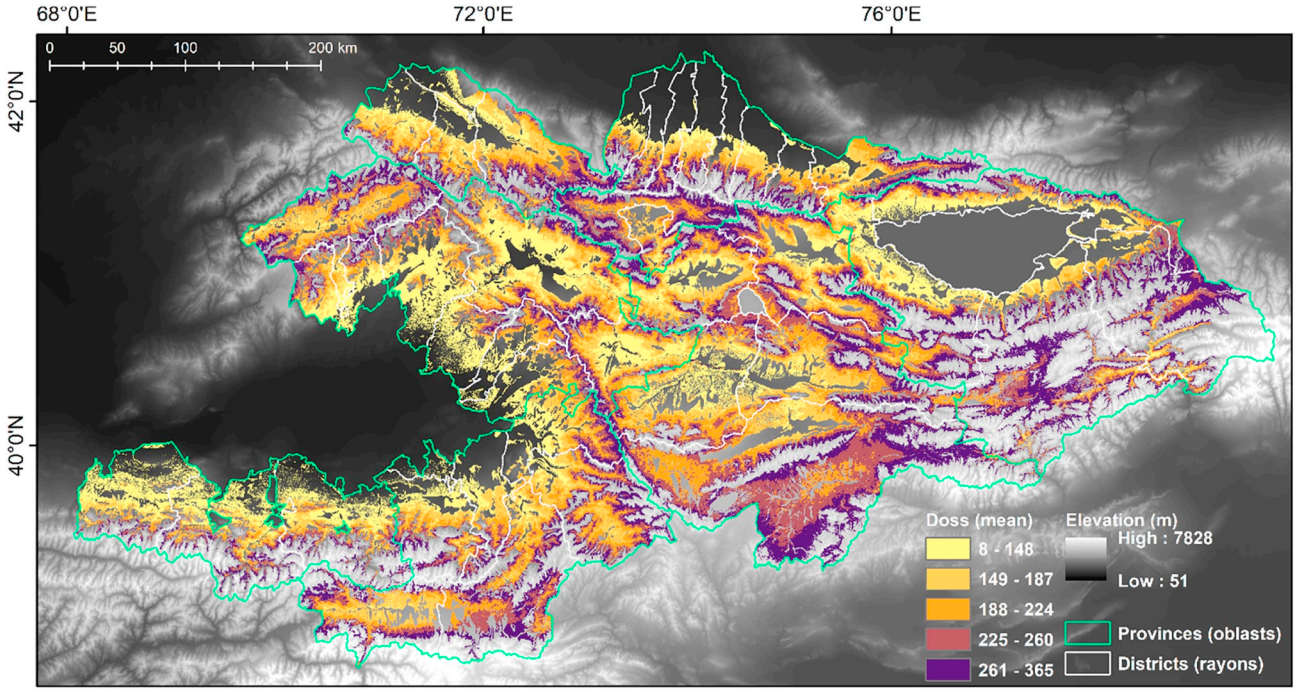

Fig. A2. Mean values of Duration of Snow Season (DoSS). Map draped over the SRTM 30 m DEM display data only for pasture land use (Projected coordinate system: Albers Conic Equal Area).

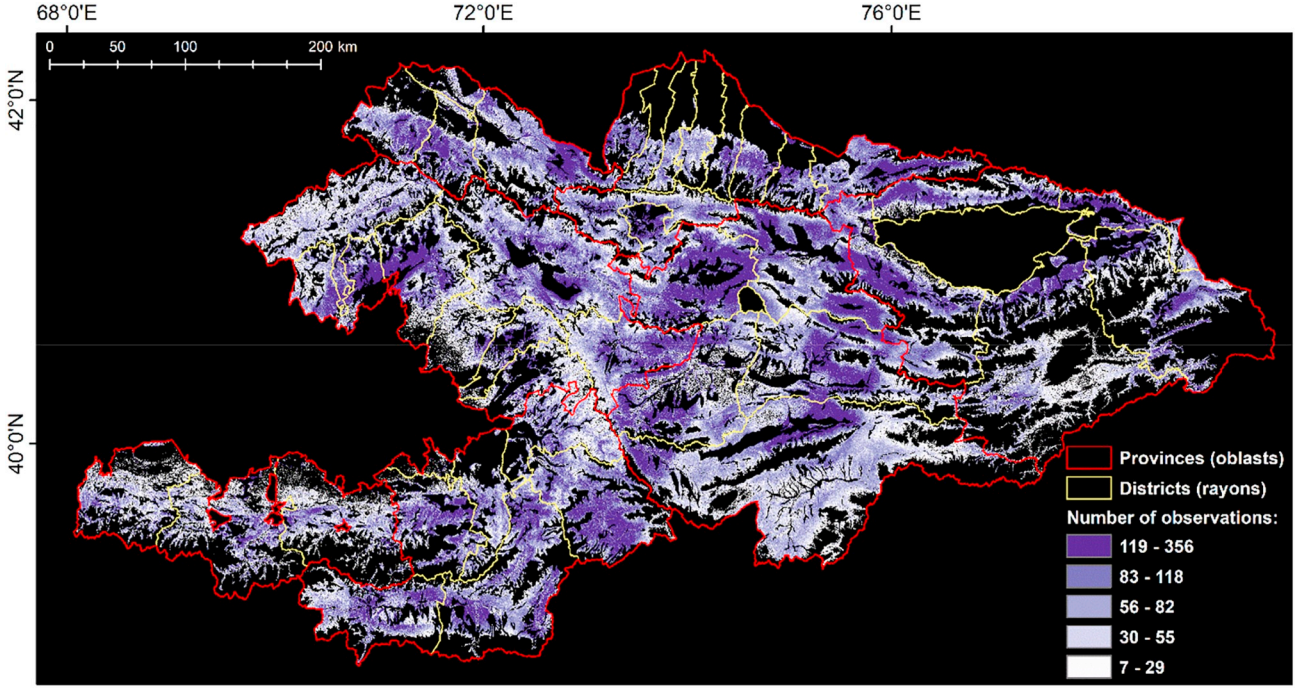

Fig. A3. Total number of data observations used for successful LSP fits over pasturelands. Classes based on quintiles. Map draped over the SRTM 30 m DEM display data only for pasture land use (Projected coordinate system: Albers Conic Equal Area).

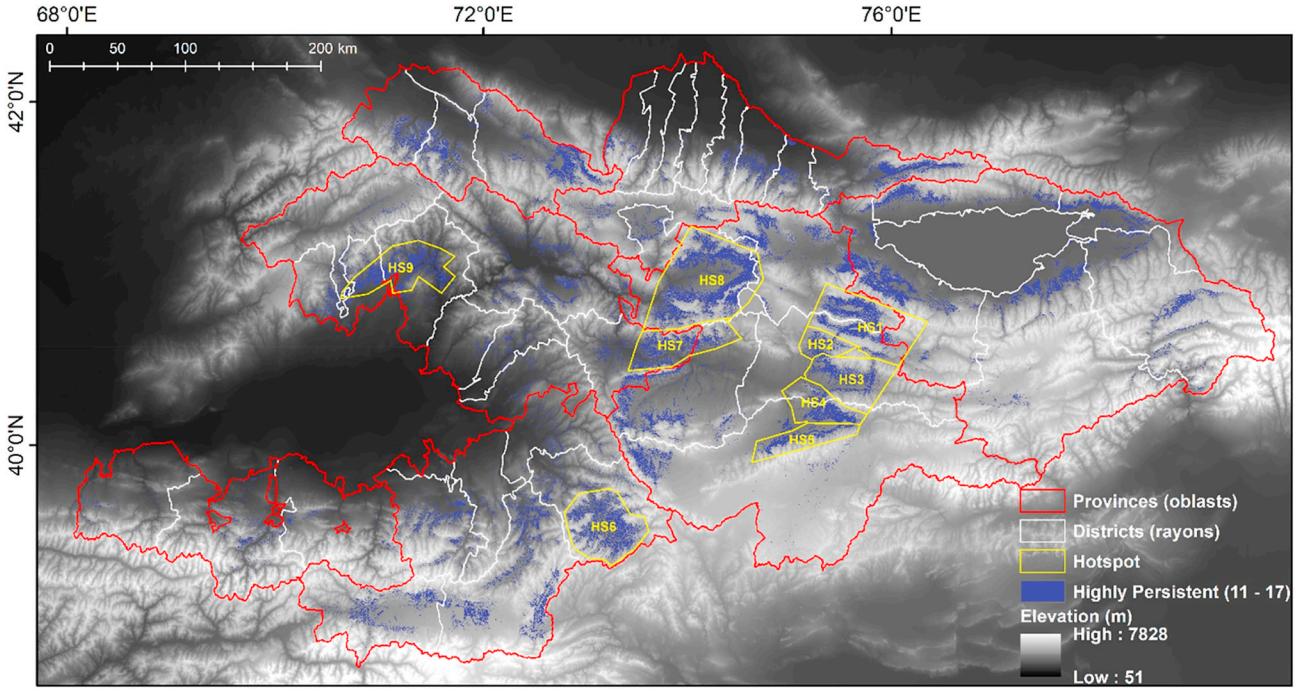

Fig. A4. Nine hotspot areas (in purple) selected based on Spearman's rank correlation results draped over the SRTM 30 m DEM (Projected coordinate system: Albers Conic Equal Area).

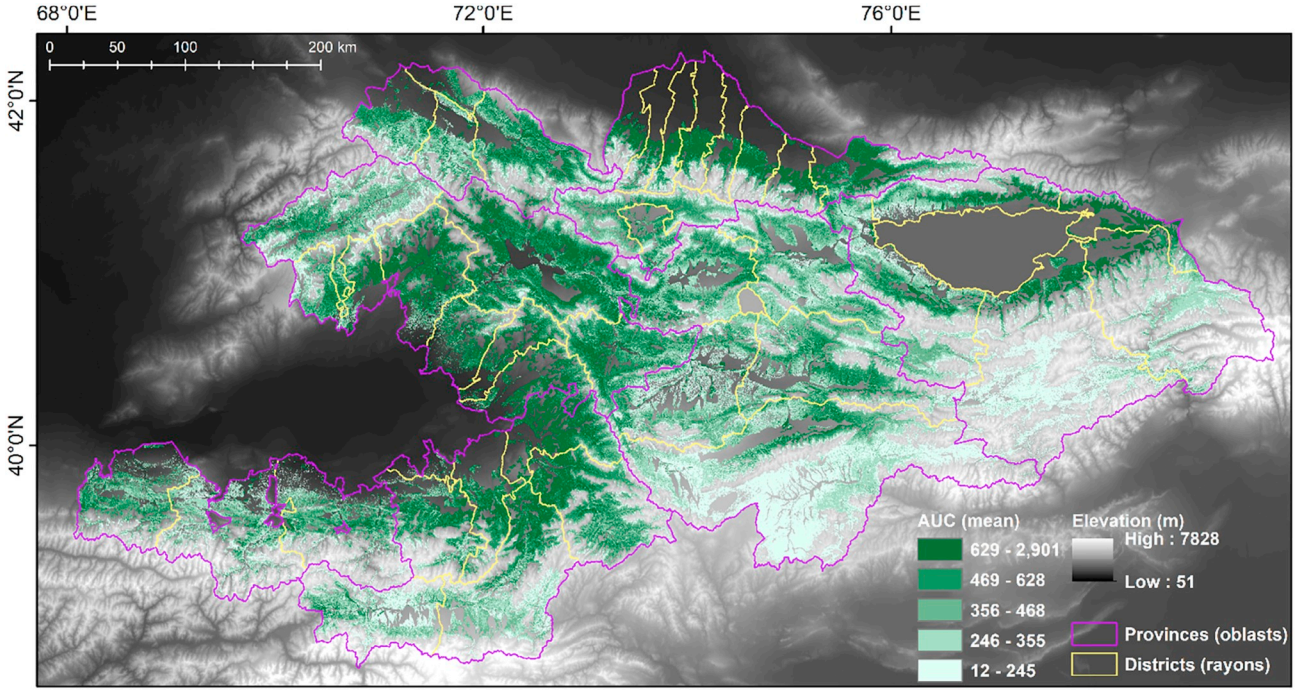

Fig. A5. Mean values of Area Under the Curve (AUC) for pasture land use areas draped over the SRTM 30 m DEM (Projected coordinate system: Albers Conic Equal Area). Classes based on quintiles.

References

Ackerman, S.A., Holz, R.E., Frey, R., Eloranta, E.W., Maddux, B.C., McGill, M., Ackerman, S.A., Holz, R.E., Frey, R., Eloranta, E.W., Maddux, B.C., McGill, M., 2008. Cloud detection with MODIS. Part II: validation. J. Atmos. Ocean. Technol. 25, 1073–1086. https://doi.org/10.1175/2007JTECHA1053.1.

Aizen, V.B., Aizen, E.M., Melack, J.M., 1995. Climate, snow cover, glaciers, and runoff in the Tien Shan. J. Am. Water Resour. Assoc. 31, 1113–1129. https://doi.org/10.1111/j.1752-1688.1995.tb03426.x.

Akimaliev, D.A., Zaurov, D.E., Eisenman, S.W., 2013. The geography, climate and vegetation of Kyrgyzstan. In: Medicinal Plants of Central Asia: Uzbekistan and Kyrgyzstan. Springer New York, New York, NY, pp. 1–4. https://doi.org/10.1007/978-1-4614-3912-7_1.

Alemu, W.G., Henebry, G.M., 2013. Land surface phenologies and seasonalities using cool earthlight in mid-latitude croplands. Environ. Res. Lett. 8, 045002. https://doi.org/10.1088/1748-9326/8/4/045002.

Allen, T.R., 2000. Topographic Normalization of Landsat Thematic Mapper Data in Three Mountain Environments. Geocarto Int. 15–22.

An, S., Zhang, X., Chen, X., Yan, D., Henebry, G.M., 2018. An exploration of terrain effects on land surface phenology across the Qinghai–Tibet Plateau using Landsat ETM+ and OLI data. Remote Sens. 10, 1069. https://doi.org/10.3390/rs10071069.

Apel, H., Abdykerimova, Z., Agalhanova, M., Baimaganbetov, A., Gavrilenko, N., Gerlitz, L., Kalashnikova, O., Unger-Shayesteh, K., Vorogushyn, S., Gafurov, A., 2018. Statistical forecast of seasonal discharge in Central Asia using observational records: development of a generic linear modelling tool for operational water resource management. Hydrol. Earth Syst. Sci. 22, 2225–2254. https://doi.org/10.5194/hess-22-2225-2018.

Armesto, J.J., Martinez, J.A., 1978. Relations between vegetation structure and slope aspect in the Mediterranean region of Chile. J. Ecol. 66, 881. https://doi.org/10.2307/2259301.

Asian Development Bank, 2010a. Central Asia Atlas of Natural Resource. Central Asian Countries Initiative for Land Management and Asian Development Bank, Manila, Philippines.

Asian Development Bank, 2010b. Central Asian countries initiative for land management (CACILM) multicountry partnership framework support project [WWW document]. URL. https://www.adb.org/projects/38464-012/main.

Azykova, E.K., 2002. Geographyical and landscape characteristics of mountain territories. In: Aidaraliev, A.A. (Ed.), Mountains of Kyrgyzstan. Technology, Bishkek.

Badano, E.I., Cavieres, L.A., Molina-Montenegro, M.A., Quiroz, C.L., 2005. Slope aspect influences plant association patterns in the Mediterranean matorral of central Chile. J. Arid Environ. 62, 93–108. https://doi.org/10.1016/J.JARIDENV.2004.10.012.

Bai, J., Shi, H., Yu, Q., Xie, Z., Li, L., Luo, G., Jin, N., Li, J., 2019. Satellite-observed vegetation stability in response to changes in climate and total water storage in Central Asia. Sci. Total Environ. 659, 862–871. https://doi.org/10.1016/J.SCITOTENV.2018.12.418.

Bennie, J., Hill, M.O., Baxter, R., Huntley, B., 2006. Influence of slope and aspect on long-term vegetation change in British chalk grasslands. J. Ecol. 94, 355–368. https://doi.org/10.1111/j.1365-2745.2006.01104.x.

Bernauer, T., Siegfried, T., 2012. Climate change and international water conflict in Central Asia. J. Peace Res. 49, 227–239. https://doi.org/10.1177/0022343311425843.

de Beurs, K.M., Henebry, G.M., 2004. Land surface phenology, climatic variation, and institutional change: analyzing agricultural land cover change in Kazakhstan. Remote Sens. Environ. 89, 497–509. https://doi.org/10.1016/J.RSE.2003.11.006.

de Beurs, K.M., Henebry, G.M., 2008. Northern annular mode effects on the land surface phenologies of northern Eurasia. J. Clim. 21, 4257–4279. https://doi.org/10.1175/2008JCLI2074.1.

de Beurs, K.M., Henebry, G.M., 2010a. Spatio-temporal statistical methods for modelling land surface phenology. In: Hudson, I.L., Keatley, M.R. (Eds.), Phenological Research. Springer Science+Business Media B.V, Dordrecht, pp. 177–208. https://doi.org/10.1007/978-90-481-3335-2_9.

de Beurs, K.M., Henebry, G.M., 2010b. A land surface phenology assessment of the northern polar regions using MODIS reflectance time series. Can. J. Remote. Sens. 36, S87–S110. https://doi.org/10.5589/m10-021.

de Beurs, K.M., Henebry, G.M., Owsley, B.C., Sokolik, I.N., 2015. Using multiple remote sensing perspectives to identify and attribute land surface dynamics in Central Asia 2001–2013. Remote Sens. Environ. 170, 48–61. https://doi.org/10.1016/j.rse.2015.08.018.

de Beurs, K.M., Henebry, G.M., Owsley, B.C., Sokolik, I.N., 2018. Large scale climate oscillation impacts on temperature, precipitation and land surface phenology in Central Asia. Environ. Res. Lett. 13, 065018. https://doi.org/10.1088/1748-9326/aac4d0.

Bohovic, R., Dobrovolny, P., Klein, D., 2016. The spatial and temporal dynamics of remotely-sensed vegetation phenology in central Asia in the 1982–2011 period. Eur. J. Remote Sens. 49, 279–299. https://doi.org/10.5721/EuJRS20164916.

Chen, Y., Li, W., Deng, H., Fang, G., Li, Z., 2016. Changes in Central Asia's water tower: past, present and future. Sci. Rep. 6, 35458. https://doi.org/10.1038/srep35458.

Choler, P., 2015. Growth response of temperate mountain grasslands to inter-annual variations in snow cover duration. Biogeosciences 12, 3885–3897. https://doi.org/10.5194/bg-12-3885-2015.

Claverie, M., Ju, J., Masek, J.G., Dungan, J.L., Vermote, E.F., Roger, J.-C., Skakun, S.V., Justice, C., 2018. The harmonized Landsat and Sentinel-2 surface reflectance data set. Remote Sens. Environ. 219, 145–161. https://doi.org/10.1016/J.RSE.2018.09.002.

Crane, R.G., Anderson, M.R., 1984. Satellite discrimination of snow/cloud surfaces. Int. J. Remote Sens. 5, 213–223. https://doi.org/10.1080/01431168408948799.

Danielson, J.J., Gesch, D.B., 2011. Global multi-resolution terrain elevation data 2010 (GMTED2010). https://doi.org/10.3133/ofr20111073.

Dedieu, J.P., Lessard-Fontaine, A., Ravazzani, G., Cremonese, E., Shalpykova, G., Beniston, M., 2014. Shifting mountain snow patterns in a changing climate from remote sensing retrieval. Sci. Total Environ. 493, 1267–1279. https://doi.org/10.1016/J.SCITOTENV.2014.04.078.

Diaz, H.F., Grosjean, M., Graumlich, L., 2003. Climate variability and change in high elevation regions: past, present and future. Clim. Chang. 59, 1–4. https://doi.org/10.1023/A:1024416227887.

Eddy, I.M.S., Gergel, S.E., Coops, N.C., Henebry, G.M., Levine, J., Zerriffi, H., Shibkov, E., 2017. Integrating remote sensing and local ecological knowledge to monitor rangeland dynamics. Ecol. Indic. 82, 106–116. https://doi.org/10.1016/J.ECOLIND.2017.06.033.

FAO, 2015. FAOStats: Statistics Page of the Food and Agriculture Organisation (FAO). [WWW Document]. URL. http://www.fao.org/faostat/en/#data/RL.

Fieller, E.C., Hartley, H.O., Pearson, E.S., 1957. Tests for rank correlation coefficients. I. Biometrika 44, 470. https://doi.org/10.2307/2332878.

Fisher, J.I., Mustard, J.F., Vadeboncoeur, M.A., 2006. Green leaf phenology at Landsat resolution: scaling from the field to the satellite. Remote Sens. Environ. 100, 265–279. https://doi.org/10.1016/J.RSE.2005.10.022.

Foody, G.M., 2009. Classification accuracy comparison: hypothesis tests and the use of confidence intervals in evaluations of difference, equivalence and non-inferiority. Remote Sens. Environ. 113, 1658–1663. https://doi.org/10.1016/J.RSE.2009.03.014.

Frey, J., 2009. An exact multinomial test for equivalence. Can. J. Stat./La Rev. Can. Stat. https://doi.org/10.2307/25653460.

Gascoin, S., Grizonnet, M., Bouchet, M., Salgues, G., Hagolle, O., 2019. Theia Snow collection: high-resolution operational snow cover maps from Sentinel-2 and Landsat-8 data. Earth Syst. Sci. Data 11, 493–514. https://doi.org/10.5194/essd-11-493-2019.

Gong, X., Brueck, H., Giese, K.M., Zhang, L., Sattelmacher, B., Lin, S., 2008. Slope aspect has effects on productivity and species composition of hilly grassland in the Xilin River Basin, Inner Mongolia, China. J. Arid Environ. 72, 483–493. https://doi.org/10.1016/J.JARIDENV.2007.07.001.

Gonsamo, A., Chen, J.M., 2016. Circumpolar vegetation dynamics product for global change study. Remote Sens. Environ. 182, 13–26. https://doi.org/10.1016/j.rse.2016.04.022.

Goodin, D.G., Henebry, G.M., 1997. A technique for monitoring ecological disturbance in tallgrass prairie using seasonal NDVI trajectories and a discriminant function mixture model. Remote Sens. Environ. 61, 270–278. https://doi.org/10.1016/S0034-4257(97)00043-6.

Goslee, S.C., 2011. Analyzing remote sensing data in R: the landsat package. J. Stat. Softw. 43, 1–25. https://doi.org/10.18637/jss.v043.i04.

Groffman, P.M., Driscoll, C.T., Fahey, T.J., Hardy, J.P., Fitzhugh, R.D., Tierney, G.L., 2001. Colder soils in a warmer world: a snow manipulation study in a northern hardwood forest ecosystem. Biogeochemistry 56, 135–150. https://doi.org/10.1023/A:1013039830323.

Hall, D.K., Riggs, G.A., Salomonson, V.V., DiGirolamo, N.E., Bayr, K.J., 2002. MODIS snow-cover products. Remote Sens. Environ. 83, 181–194. https://doi.org/10.1016/S0034-4257(02)00095-0.

Henebry, G.M., 2013. Phenologies of North American grasslands and grasses. In: Schwartz, M.D. (Ed.), Phenology: An Integrative Environmental Science. Springer Netherlands, Dordrecht, pp. 197–210. https://doi.org/10.1007/978-94-007-6925-0.

Henebry, G.M., de Beurs, K.M., 2013. Remote sensing of land surface phenology: a prospectus. In: Phenology: An Integrative Environmental Science. Springer Netherlands, Dordrecht, pp. 385–411. https://doi.org/10.1007/978-94-007-6925-0_21.

Hijioka, Y., Lin, E., Pereira, J.J., Corlett, R.T., Cui, X., Insarov, G.E., Lasco, R.D., Lindgren, E., Surjan, A., 2014. Asia.

Huete, A., Justice, C., Van Leeuwen, W., 1999. MODIS Vegetation Index (MOD13) Algorithm Theoretical Basis Document, Ver. 3.

Immerzeel, W.W., van Beek, L.P.H., Bierkens, M.F.P., 2010. Climate change will affect the Asian water towers. Science 328, 1382–1385. https://doi.org/10.1126/science.1183188.

Julitta, T., Cremonese, E., Migliavacca, M., Colombo, R., Galvagno, M., Siniscalco, C., Rossini, M., Fava, F., Cogliati, S., Morra di Cella, U., Menzel, A., 2014. Using digital camera images to analyse snowmelt and phenology of a subalpine grassland. Agric. For. Meteorol. 198–199, 116–125. https://doi.org/10.1016/J.AGRFORMET.2014.08.007.

Kariyeva, J., van Leeuwen, W.J.D., 2011. Environmental drivers of NDVI-based vegetation phenology in central Asia. Remote Sens. 3, 203–246. https://doi.org/10.3390/rs3020203.

Karnieli, A., Bayarjargal, Y., Bayasgalan, M., Mandakh, B., Dugarjav, C., Burgheimer, J., Khudulmur, S., Bazha, S.N., Gunin, P.D., 2013. Do vegetation indices provide a reliable indication of vegetation degradation? A case study in the Mongolian pastures. Int. J. Remote Sens. 34, 6243–6262. https://doi.org/10.1080/01431161.2013.793865.

Krehbiel, C., Henebry, G., 2016. A comparison of multiple datasets for monitoring thermal time in urban areas over the U.S. upper Midwest. Remote Sens. 8, 297. https://doi.org/10.3390/rs8040297.

Krehbiel, C., Zhang, X., Henebry, G., 2017. Impacts of thermal time on land surface phenology in urban areas. Remote Sens. 9, 499. https://doi.org/10.3390/rs9050499.

Kulikov, M., Schickhoff, U., 2017. Vegetation and climate interaction patterns in Kyrgyzstan: spatial discretization based on time series analysis. Erdkunde 71, 143–165. https://doi.org/10.3112/erdkunde.2017.02.04.

Lehmann, E.L., D'Abrera, H.J.M., 2006. Nonparametrics: Statistical Methods Based on Ranks. Springer.

Lioubimtseva, E., Henebry, G.M., 2009. Climate and environmental change in arid Central Asia: impacts, vulnerability, and adaptations. J. Arid Environ. 73, 963–977. https://doi.org/10.1016/j.jaridenv.2009.04.022.

Liu, M., Che, Y., Jiao, J., Li, L., Jiang, X., 2019. Exploring the community phylogenetic structure along the slope aspect of subalpine meadows in the eastern Qinghai–Tibetan Plateau, China. Ecol. Evol. 9, 5270–5280. https://doi.org/10.1002/ece3.5117.

Liu, Y., Hill, M.J., Zhang, X., Wang, Z., Richardson, A.D., Hufkens, K., Filippa, G., Baldocchi, D.D., Ma, S., Verfaillie, J., Schaaf, C.B., 2017. Using data from Landsat, MODIS, VIIRS and PhenoCams to monitor the phenology of California oak/grass savanna and open grassland across spatial scales. Agric. For. Meteorol. 237–238, 311–325. https://doi.org/10.1016/J.AGRFORMET.2017.02.026.

Lu, L., Guo, H., Kuenzer, C., Klein, I., Zhang, L., Li, X., 2014. Analyzing phenological changes with remote sensing data in Central Asia. IOP Conf. Ser. Earth Environ. Sci.

17, 012005. https://doi.org/10.1088/1755-1315/17/1/012005.
Luo, M., Liu, T., Meng, F., Duan, Y., Bao, A., Frankl, A., De Maeyer, P., 2018. Spatiotemporal characteristics of future changes in precipitation and temperature in Central Asia. Int. J. Climatol. https://doi.org/10.1002/joc.5901.
Måren, I.E., Karki, S., Prajapati, C., Yadav, R.K., Shrestha, B.B., 2015. Facing north or south: does slope aspect impact forest stand characteristics and soil properties in a semiarid trans-Himalayan valley? J. Arid Environ. 121, 112–123. https://doi.org/10.1016/J.JARIDENV.2015.06.004.
Marshall, A.M., Link, T.E., Abatzoglou, J.T., Flerchinger, G.N., Marks, D.G., Tedrow, L., 2019. Warming alters hydrologic heterogeneity: simulated climate sensitivity of hydrology-based microrefugia in the snow-to-rain transition zone. Water Resour. Res. 55, 2122–2141. https://doi.org/10.1029/2018WR023063.
Matsushita, B., Yang, W., Chen, J., Onda, Y., Qiu, G., 2007. Sensitivity of the enhanced vegetation index (EVI) and normalized difference vegetation index (NDVI) to topographic effects: a case study in high-density cypress Forest. Sensors 7, 2636–2651. https://doi.org/10.3390/s7112636.
Melaas, E.K., Friedl, M.A., Zhu, Z., 2013. Detecting interannual variation in deciduous broadleaf forest phenology using Landsat TM/ETM + data. Remote Sens. Environ. 132, 176–185. https://doi.org/10.1016/J.RSE.2013.01.011.
Melaas, E.K., Sulla-Menashe, D., Gray, J.M., Black, T.A., Morin, T.H., Richardson, A.D., Friedl, M.A., 2016. Multisite analysis of land surface phenology in North American temperate and boreal deciduous forests from Landsat. Remote Sens. Environ. 186, 452–464. https://doi.org/10.1016/j.rse.2016.09.014.
Monson, R.K., Lipson, D.L., Burns, S.P., Turnipseed, A.A., Delany, A.C., Williams, M.W., Schmidt, S.K., 2006. Winter forest soil respiration controlled by climate and microbial community composition. Nature 439, 711–714. https://doi.org/10.1038/nature04555.
Moreira, E.P., Valeriano, M., Sanches, I., Formaggio, A.R., 2016. Topographic effect on spectral vegetation indices from Landsat TM data: is topographic correction necessary? Bol. Ciências Geodésicas 22, 95–107. https://doi.org/10.1590/S1982-21702016000100006.
Moritz, S., Bartz-Beielstein, T., 2017. imputeTS: time series missing value imputation in R. [WWW Document]. R J. 9.1. URL. https://journal.r-project.org/archive/2017/RJ-2017-009/RJ-2017-009.pdf.
NASA JPL, 2013. NASA Shuttle Radar Topography Mission Global 1 Arc Second [Data Set]. WWW Document. NASA EOSDIS L. Process. DAAChttps://doi.org/10.5067/MEaSUREs/SRTM/SRTMGL1.003.
Nguyen, L.H., Henebry, G.M., 2019. Characterizing land use/land cover using multisensor time series from the perspective of land surface phenology. Remote Sens. 11, 1677. https://doi.org/10.3390/rs11141677.
Nguyen, L.H., Joshi, D.R., Clay, D.E., Henebry, G.M., 2018. Characterizing land cover/land use from multiple years of Landsat and MODIS time series: a novel approach using land surface phenology modeling and random forest classifier. Remote Sens. Environ. https://doi.org/10.1016/J.RSE.2018.12.016.
Paudel, K.P., Andersen, P., 2013. Response of rangeland vegetation to snow cover dynamics in Nepal Trans Himalaya. Clim. Chang. 117, 149–162. https://doi.org/10.1007/s10584-012-0562-x.
Pepin, N., Bradley, R.S., Diaz, H.F., Baraer, M., Caceres, E.B., Forsythe, N., Fowler, H., Greenwood, G., Hashmi, M.Z., Liu, X.D., Miller, J.R., Ning, L., Ohmura, A., Palazzi, E., Rangwala, I., Schöner, W., Severskiy, I., Shahgedanova, M., Wang, M.B., Williamson, S.N., Yang, D.Q., 2015. Elevation-dependent warming in mountain regions of the world. Nat. Clim. Chang. 5, 424–430. https://doi.org/10.1038/nclimate2563.
Pervez, M.S., Henebry, G.M., 2015. Spatial and seasonal responses of precipitation in the Ganges and Brahmaputra river basins to ENSO and Indian Ocean dipole modes: implications for flooding and drought. Nat. Hazards Earth Syst. Sci. 15, 147–162. https://doi.org/10.5194/nhess-15-147-2015.
Petersky, R.S., Shoemaker, K.T., Weisberg, P.J., Harpold, A.A., 2019. The sensitivity of snow ephemerality to warming climate across an arid to montane vegetation gradient. Ecohydrology 12, e2060. https://doi.org/10.1002/eco.2060.
Qiao, D., Wang, N., 2019. Relationship between winter snow cover dynamics, climate and spring grassland vegetation phenology in Inner Mongolia, China. ISPRS Int. J. Geo-Information 8, 42. https://doi.org/10.3390/ijgi8010042.
Reyer, C.P.O., Otto, I.M., Adams, S., Albrecht, T., Baarsch, F., Cartsburg, M., Coumou, D., Eden, A., Ludi, E., Marcus, R., Mengel, M., Mosello, B., Robinson, A., Schleussner, C.F., Serdeczny, O., Stagl, J., 2017. Climate change impacts in Central Asia and their implications for development. Reg. Environ. Chang. 17, 1639–1650. https://doi.org/10.1007/s10113-015-0893-z.
Riaño, D., Chuvieco, E., Salas, J., Aguado, I., 2003. Assessment of different topographic corrections in Landsat-TM data for mapping vegetation types. IEEE Trans. Geosci. Remote Sens. 41. https://doi.org/10.1109/TGRS.2003.811693.
Riggs, G.A., Hall, D.K., 2004. Snow Mapping with the MODIS Aqua Instrument. (61st East. Snow Conf).
Riggs, G.A., Hall, D.K., 2015. MODIS Snow Products Collection 6 User Guide. NSIDC. https://nsidc.org/sites/nsidc.org/files/files/MODIS-snow-user-guide-C6.pdf.
Rossi, M., Niedrist, G., Asam, S., Tonon, G., Tomelleri, E., Zebisch, M., Rossi, M., Niedrist, G., Asam, S., Tonon, G., Tomelleri, E., Zebisch, M., 2019. A comparison of the signal from diverse optical sensors for monitoring Alpine grassland dynamics. Remote Sens. 11, 296. https://doi.org/10.3390/rs11030296.
Roy, D.P., Kovalskyy, V., Zhang, H.K., Vermote, E.F., Yan, L., Kumar, S.S., Egorov, A., 2016. Characterization of Landsat-7 to Landsat-8 reflective wavelength and normalized difference vegetation index continuity. Remote Sens. Environ. 185, 57–70. https://doi.org/10.1016/J.RSE.2015.12.024.
Schillhorn Van Veen, T.W., 1995. The Kyrgyz Sheep Herders at a Crossroads. Overseas Dev. Institute. Pastor. Dev. Netw. Ser.
Schimel, J.P., Bilbrough, C., Welker, J.M., 2004. Increased snow depth affects microbial activity and nitrogen mineralization in two Arctic tundra communities. Soil Biol. Biochem. 36, 217–227. https://doi.org/10.1016/J.SOILBIO.2003.09.008.
Sorg, A., Bolch, T., Stoffel, M., Solomina, O., Beniston, M., 2012. Climate change impacts on glaciers and runoff in Tien Shan (Central Asia). Nat. Clim. Chang. 2. https://doi.org/10.1038/NCLIMATE1592.
Sternberg, M., Shoshany, M., 2001. Influence of slope aspect on Mediterranean woody formations: comparison of a semiarid and an arid site in Israel. Ecol. Res. 16, 335–345. https://doi.org/10.1046/j.1440-1703.2001.00393.x.
Still, C.J., Pau, S., Edwards, E.J., 2014. Land surface skin temperature captures thermal environments of C 3 and C 4 grasses. Glob. Ecol. Biogeogr. 3, 286–296. https://doi.org/10.1111/geb.12121.
Telwala, Y., Brook, B.W., Manish, K., Pandit, M.K., 2013. Climate-induced elevational range shifts and increase in plant species richness in a Himalayan biodiversity epicentre. PLoS One 8, e57103. https://doi.org/10.1371/journal.pone.0057103.
Thompson, L.G., 2000. Ice core evidence for climate change in the tropics: implications for our future. Quat. Sci. Rev. 19, 19–35.
Tomaszewska, M.A., Henebry, G.M., 2018. Changing snow seasonality in the highlands of Kyrgyzstan. Environ. Res. Lett. 13, 065006. https://doi.org/10.1088/1748-9326/aabd6f.
Tucker, C.J., 1979. Red and photographic infrared linear combinations for monitoring vegetation. Remote Sens. Environ. 8, 127–150. https://doi.org/10.1016/0034-4257(79)90013-0.
USGS EROS, 2017. Landsat Collection 1 Level 1 Product Definition. (Sioux Falls, SD).
Vázquez-Jiménez, R., Romero-Calcerrada, R., Ramos-Bernal, R., Arrogante-Funes, P., Novillo, C., 2017. Topographic correction to Landsat imagery through slope classification by applying the SCS + C method in mountainous forest areas. ISPRS Int. J. Geo-Information 6, 287. https://doi.org/10.3390/ijgi6090287.
Viña, A., Henebry, G.M., 2005. Spatio-temporal change analysis to identify anomalous variation in the vegetated land surface: ENSO effects in tropical South America. Geophys. Res. Lett. 32, 1–5. https://doi.org/10.1029/2005GL023407.
Wan, Y., Gao, Q., Li, Y., Qin, X., Zhang, W., Ma, X., Liu, S., 2014. Change of snow cover and its impact on Alpine vegetation in the source regions of large Rivers on the Qinghai-Tibetan plateau. Arctic, Antarct. Alp. Res. 46, 632–644. https://doi.org/10.1657/1938-4246-46.3.632.
Wan, Z., Hook, S., Hulley, G., 2015. MOD11A2 MODIS/Terra Land Surface Temperature/Emissivity 8-Day L3 Global 1km SIN Grid V006.
Wang, L., Li, Z., Wang, F., Edwards, R., 2014. Glacier shrinkage in the Ebinur lake basin, Tien Shan, China, during the past 40 years. J. Glaciol. 60, 245–254. https://doi.org/10.3189/2014JoG13J023.
Wang, X., Wu, C., Peng, D., Gonsamo, A., Liu, Z., 2018. Snow cover phenology affects alpine vegetation growth dynamics on the Tibetan Plateau: satellite observed evidence, impacts of different biomes, and climate drivers. Agric. For. Meteorol. 256–257, 61–74. https://doi.org/10.1016/J.AGRFORMET.2018.03.004.
Watson, C.J., Restrepo-Coupe, N., Huete, A.R., 2019. Multi-scale phenology of temperate grasslands: improving monitoring and management with near-surface phenocams. Front. Environ. Sci. 7, 14. https://doi.org/10.3389/fenvs.2019.00014.
Welker, J.M., Fahnestock, J.T., Sullivan, P.F., Chimner, R.A., 2005. Leaf mineral nutrition of Arctic plants in response to warming and deeper snow in northern Alaska. Oikos 109, 167–177. https://doi.org/10.1111/j.0030-1299.2005.13264.x.
Wellek, S., 2010. Testing Statistical Hypotheses of Equivalence and Noninferiority, Second Edition, 2nd ed. Chapman and Hall/CRC, New York City. https://doi.org/10.1201/EBK1439808184.
Westergaard-Nielsen, A., Lund, M., Pedersen, S.H., Schmidt, N.M., Klosterman, S., Abermann, J., Hansen, B.U., 2017. Transitions in high-Arctic vegetation growth patterns and ecosystem productivity tracked with automated cameras from 2000 to 2013. Ambio 46, 39–52. https://doi.org/10.1007/s13280-016-0864-8.
WorldBank, 2018. Kyrgyzstan; Population 2018. [WWW Document]. URL. https://data.worldbank.org/country/kyrgyz-republic.
Wright, C.K., de Beurs, K.M., Henebry, G.M., 2014. Land surface anomalies preceding the 2010 Russian heat wave and a link to the North Atlantic oscillation. Environ. Res. Lett. 9, 124015. https://doi.org/10.1088/1748-9326/9/12/124015.
Xenarios, S., Gafurov, A., Schmidt-Vogt, D., Sehring, J., Manandhar, S., Hergarten, C., Shigaeva, J., Foggin, M., 2018. Climate change and adaptation of mountain societies in Central Asia: uncertainties, knowledge gaps, and data constraints. Reg. Environ. Chang. 1–14. https://doi.org/10.1007/s10113-018-1384-9.
Xie, J., Kneubühler, M., Garonna, I., Notarnicola, C., De Gregorio, L., De Jong, R., Chimani, B., Schaepman, M.E., 2017. Altitude-dependent influence of snow cover on alpine land surface phenology. J. Geophys. Res. Biogeosci. 122, 1107–1122. https://doi.org/10.1002/2016JG003728.
Xie, J., Kneubühler, M., Garonna, I., de Jong, R., Notarnicola, C., De Gregorio, L., Schaepman, M.E., 2018. Relative influence of timing and accumulation of snow on alpine land surface phenology. J. Geophys. Res. 123, 561–576. https://doi.org/10.1002/2017JG004099.
Xue, R., Yang, Q., Miao, F., Wang, X., Shen, Y., 2018. Slope aspect influences plant biomass, soil properties and microbial composition in alpine meadow on the Qinghai-Tibetan plateau. J. Soil Sci. Plant Nutr. 18https://doi.org/10.4067/S0718-95162018005000101. 0–0.
Yan, D., Scott, R.L., Moore, D.J.P., Biederman, J.A., Smith, W.K., 2019. Understanding the

relationship between vegetation greenness and productivity across dryland ecosystems through the integration of PhenoCam, satellite, and eddy covariance data. Remote Sens. Environ. 223, 50–62. https://doi.org/10.1016/j.rse.2018.12.029.
Yeo, S., Kim, W., Kim, K., 2017. Eurasian snow cover variability in relation to warming trend and Arctic Oscillation. Clim. Dyn. 48, 499–511. https://doi.org/10.1007/s00382-016-3089-4.
Yu, X., Zhao, Y., Ma, X., Yao, J., Li, H., 2018. Projected changes in the annual cycle of precipitation over central Asia by CMIP5 models. Int. J. Climatol. 38, 5589–5604. https://doi.org/10.1002/joc.5765.
Yu, Z., Liu, S., Wang, J., Sun, P., Liu, W., Hartley, D.S., 2013. Effects of seasonal snow on the growing season of temperate vegetation in China. Glob. Chang. Biol. 19, 2182–2195. https://doi.org/10.1111/gcb.12206.
Zhumanova, M., Wrage-Mönnig, N., Darr, D., 2016. Farmers' decision-making and land use changes in Kyrgyz Agropastoral systems. Mt. Res. Dev. 36, 506–517. https://doi.org/10.1659/MRD-JOURNAL-D-16-00030.1.
Zhumanova, M., Mönnig, C., Hergarten, C., Darr, D., Wrage-Mönnig, N., 2018. Assessment of vegetation degradation in mountainous pastures of the Western Tien-Shan, Kyrgyzstan, using eMODIS NDVI. Ecol. Indic. 95, 527–543. https://doi.org/10.1016/j.ecolind.2018.07.060.